②

AFWAL-TR-88-3050

AN ELLIPTIC GRID GENERATION METHOD FOR CROPPED DELTA WINGS

James P. Sirbaugh
Aerodynamics & Airframe Branch
Aeromechanics Division

AD-A199 462

July 1988

Final Report for Period March 1985 - November 1986

DTIC
ELECTED
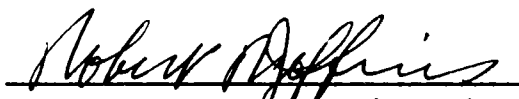SEP 2 9 1988
S
H
D

88 9 29 017

NOTICE

When Government drawings, specifications, or other data are used for any purpose other than in connection with a definitely Government-related procurement, the United States Government incurs no responsibility or any obligation whatsoever. The fact that the Government may have formulated or in any way supplied the said drawings, specifications, or other data, is not to be regarded by implication, or otherwise in any manner construed, as licensing the holder, or any other person or corporation; or as conveying any rights or permission to manufacture, use, or sell any patented invention that may in any way be related thereto.

This report has been reviewed by the Office of Public Affairs (ASD/PA) and is releasable to the National Technical Information Service (NTIS). At NTIS, it will be available to the general public, including foreign nations.

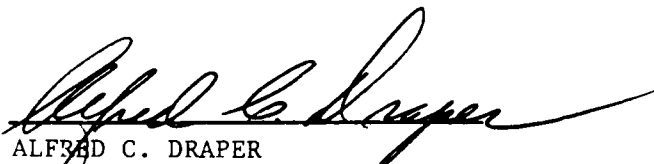This technical report has been reviewed and is approved for publication.

J.R. SIRBAUGH
Aeronautical Engineer

ROBERT R. JEFFRIES, Acting Chief
Aerodynamics & Airframe Branch
Aeromechanics Division

FOR THE COMMANDER

ALFRED C. DRAPER
Asst for Research & Technology
Aeromechanics Division
Flight Dynamics Laboratory

If your address has changed, if you wish to be removed from our mailing list, or if the addressee is no longer employed by your organization, please notify AFWAL/FIMM, WPAFB OH 45433-6553 to help us maintain a current mailing list.

Copies of this report should not be returned unless it is required by security considerations, contractual obligations, or notice on a specific document.

REPORT DOCUMENTATION PAGE

1a REPORT SECURITY CLASSIFICATION Unclassified		1b RESTRICTIVE MARKINGS			
2a. SECURITY CLASSIFICATION AUTHORITY		3. DISTRIBUTION/AVAILABILITY OF REPORT Approved for public release; distribution unlimited.			
2b DECLASSIFICATION/DOWNGRADING SCHEDULE					
4 PERFORMING ORGANIZATION REPORT NUMBER(S) AFWAL-TR-88-3050		5. MONITORING ORGANIZATION REPORT NUMBER(S)			
6a. NAME OF PERFORMING ORGANIZATION Flight Dynamics Laboratory AFWAL/AFSC	6b. OFFICE SYMBOL (If applicable) AFWAL/FIMM	7a. NAME OF MONITORING ORGANIZATION			
6c. ADDRESS (City, State, and ZIP Code) Wright-Patterson Air Force Base OH 45433-6553		7b. ADDRESS (City, State, and ZIP Code)			
8a. NAME OF FUNDING/SPONSORING ORGANIZATION	8b. OFFICE SYMBOL (If applicable) AFWAL/FIMM	9. PROCUREMENT INSTRUMENT IDENTIFICATION NUMBER			
8c. ADDRESS (City, State, and ZIP Code)		10. SOURCE OF FUNDING NUMBERS			

		PROGRAM ELEMENT NO.	PROJECT NO.	TASK NO	WORK UNIT ACCESSION NO.
		2404	10	A1	

11 TITLE (Include Security Classification)

An Elliptic Grid Generation Method for Cropped Delta Wings

12. PERSONAL AUTHOR(S)
Sirbaugh, James R.

13a. TYPE OF REPORT Final Report	13b. TIME COVERED FROM Mar 85 TO Nov 86	14. DATE OF REPORT (Year, Month, Day) 1988 July	15. PAGE COUNT 56

16. SUPPLEMENTARY NOTATION

17. COSATI CODES			18. SUBJECT TERMS (Continue on reverse if necessary and identify by block number)
FIELD	GROUP	SUB-GROUP	Grid Generation, Euler, CFD, Delta Wings, FLO57, Vortex Flow
01	01		
02	02		

19. ABSTRACT (Continue on reverse if necessary and identify by block number)

The solution of the Euler equations for aircraft flow fields involves two major problems: grid generation and flow equation solution. A grid must be generated for each new configuration to be studied. The grid must accurately model the configuration surface geometry and provide sufficient grid resolution in the region around the configuration to capture the flow details. Grid generation methods should be tailored according to both the physics of the flow and the flow equation solution method. The primary flow characteristic of the delta wing is the leading-edge separation that rolls up into a vortex. The vortex position, size and strength are dependent on many factors, one of which is the leading-edge shape. The leading-edge grid must be fine enough to permit the flow solver to capture the flow gradients contributing to leading-edge separation in order to accurately predict vortex core position and strength. The Euler equation solver used in this work is FLO57. While FLO57 has previously been applied to delta wing configuration, the built-in grid generation in FLO57 is inadequate for delta wings. A few aspects of FLO57 should be kept in mind when considering

20 DISTRIBUTION/AVAILABILITY OF ABSTRACT [X] UNCLASSIFIED/UNLIMITED ☐ SAME AS RPT ☐ DTIC USERS	21. ABSTRACT SECURITY CLASSIFICATION Unclassified	
22a. NAME OF RESPONSIBLE INDIVIDUAL D. W. Kinsey	22b. TELEPHONE (Include Area Code) (513) 255-2481	22c. OFFICE SYMBOL AFWAL/FIMM

DD Form 1473, JUN 86   Previous editions are obsolete.   SECURITY CLASSIFICATION OF THIS PAGE

19. a grid topology to be coupled to the Euler equation solver. A finite-volume and central-difference scheme is used by the method. The finite-volume method does not require grid lines to be continuous in slope, or orthogonal; thus the grid can be generated by a variety of ways, including those which do not directly enforce orthogonality. Boundary conditions are applied in the FLO57 Euler method in a variety of ways, some of which require an extrapolation of interior flow variables to the grid boundaries. Although the boundary conditions do not explicitly require orthogonal grids, it is reasonable, when considering the boundary condition extrapolation, that orthogonality at the grid boundaries would improve the code's accuracy.

FOREWORD

This in-house effort was accomplished under Work Unit 240410A1, entitled "Aerodynamic Design and Analysis Methods." The work reported herein was performed during the period March 1985 to November 1986 under the direction of the author, James R. Sirbaugh (AFWAL/FIMM).

Accession For	
NTIS GRA&I	☑
DTIC TAB	☐
Unannounced	☐
Justification	
By	
Distribution/	
Availability Codes	
Dist	Avail and/or Special
A-1	

TABLE OF CONTENTS

LIST OF FIGURES

SECTION I

INTRODUCTION

The solution of the Euler equations for aircraft flow fields involves two major problems: grid generation and flow equation solution. A grid must be generated for each new configuration to be studied. The grid must accurately model the configuration surface geometry and provide sufficient grid resolution in the region around the configuration to capture the flow details. Due to current computer speed and memory limits, a computational aerodynamics code must be limited in the number of grid points it uses, and therefore the grid point locations must be chosen carefully. The following pages describe the development and application of a delta wing grid topology.

Grid generation methods should be tailored according to both the physics of the flow and the flow equation solution method. The primary flow characteristic of the delta wing is the leading-edge separation that rolls up into a vortex. The vortex position, size and strength are dependent on many factors, one of which is the leading-edge shape. A sharp leading edge will generally produce a vortex originating at the edge, while a round leading edge may produce a separation point more inboard on the upper surface thus increasing the strength of the vortex. The leading-edge grid must be fine enough to permit the flow solver to capture the flow gradients contributing to leading-edge separation in order to accurately predict vortex core position and strength. Downstream of the wing, the vortex core will diffuse to a degree, and may even burst or breakdown. If a computational method, such as an Euler solver, is going to predict the occurrence of vortex burst, the downsteam grid must adequately resolve the vortex flow. Even for cases where burst is not a consideration, the grid immediately downstream of the wing must be dense enough to accurately predict the trailing-edge flow field.

1

The Euler equation solver used in this work is FLO57 (Ref. 1). While FLO57 has previously been applied to delta wing configuration, the built-in grid generation in FLO57 is inadequate for delta wings. The grid does not model the wingtip and produces a downstream grid which is highly skewed for configurations with large leading-edge sweeps. A few aspects of FLO57 should be kept in mind when considering a grid topology to be coupled to the Euler equation solver. A finite-volume and central-difference scheme is used by the method. The finite-volume method does not require grid lines to be continuous in slope, or orthogonal; thus, the grid can be generated by a variety of ways, including those which do not directly enforce orthogonality. The total grid may also be broken up into several regions and each region generated separately, as long as grid lines are continuous across region boundaries. A highly skewed grid, however, will generate inaccurate flow field solutions; i.d., a fact that must be kept in mind when considering nonorthogonal grids.

The central-difference scheme is used to calculate mass, momentum, and energy fluxes across each grid cell face by averaging the flow variable values adjacent to the cell face. This calculation procedure assumes that the distance between the cell face, where the flux is calculated, and the cell center, where the flow variables are calculated, is approximately the same for neighboring cells. Should the grid point spacing vary extremely rapidly or in a nonsmooth fashion, the simple averaging of variables will produce an inaccurate approximation to the cell face flux. The far-field grid region typically has rapid grid stretching; however, the flow solution accuracy is not significantly degraded in this region due to the nearly uniform flow at the far field.

Boundary conditions are applied in the FLO57 Euler method in a variety of ways, some of which require an extrapolation of interior flow variables to the

grid boundaries. Although the boundary conditions do not explicitly require orthogonal grids, it is reasonable, when considering the boundary condition extrapolation, that orthogonality at the grid boundaries would improve the code's accuracy.

SECTION II

GRID TOPOLOGY

The new delta wing grid developed during this effort is based on a previously developed two-dimensional (2-D) grid topology for equilateral triangles (Ref. 2), Fig. 1. The leading edge and wingtip are considered to be a single side of the equilateral-triangle grid. The singularity point is positioned on the root chord and therefore should not be in any strong flow gradients region for most problems of interest. Figures 2a-c show the wing surface topology for a 65° leading-edge sweep, cropped delta wing. This topology permits a uniform grid point spacing and cell size along the entire length of the leading edge. Grid cells can be clustered forward on the wing by moving the singularity point forward, thus permitting adequate grid resolution to capture the strong flow gradients in the apex region.

The new delta wing grid is intended primarily for use with the FLO57 Euler analysis code. In order to couple the new grid topology to the existing FLO57 Euler code with as few changes to FLO57 as possible, the following grid index system was adopted. The grid lines that wrap across the wing surface and around the leading edge of the wing will be referred to as the I-varying (K constant) grid lines. (See 3a.) The I = 1 grid points are located on the wing's lower surface root chord. The $I = I_{max}$ grid points are located on the wing's upper surface root chord. The line forming the forward part of the root chord starts at the lower surface singularity, varies in I and moves forward around the leading edge and proceeds aft to the upper surface singularity. This grid line is varying in I and has a constant K value of one. The K-varying family of curves start at the forward plane of symmetry with a value of one and follows paths aft to the downstream exit plane. Thus, the wing's trailing edge is formed by a grid line varying in I and a constant K value.

4

To form a three-dimensional (3-D) grid, the C-H grid topology in FLO57 was partially merged to the delta wing grid topology to form a wrapped O-H grid. Each O wrap followed an I-varying grid line, with the O wraps being almost spanwise cuts near the wing's trailing edge. A typical O wrap from the 3-D grid is shown in Figs. 4a and b. The wing surface was formed by the J = 1 grid points and the J_{max} grid points form the outer shell of the 3-D grid. The delta wing grid topology is not totally new and is easy to follow if the viewer considers the grid to be a series of 2-D O grids stacked together to form the 3-D grid. Figures 3a and b show the plane-of-symmetry grid with index directions indicated.

To couple the 3-D delta wing grid to FLO57, the boundary conditions to be applied on each face of the 3-D computational cube must be determined. The J = 1 side is the wing surface for all K values less than or equal to the K value of the wing's trailing edge. For J = 1 and K values greater than K trailing edge value, the grid collapses to a slit line and a flow through boundary condition is used. The J = J_{max} side is the far-field grid and appropriate in-flow/out-flow boundary conditions apply. The plane-of-symmetry grid is formed by the I = 1, I = I_{max} and the K = 1 sides of the computational grid. The only remaining side of the computational space is the K = K_{max} side and this is the downstream boundary grid where appropriate out-flow boundary conditions are applied.

GRID GENERATION

The delta wing grid used in the Euler computation was developed in three phases: 2-D boundary grids, 3-D interior grid, and algebraic downstream grid. The 2-D grids are the six sides of the 3-D grid, consisting of the wing upper and lower surfaces, symmetry plane (3 sides), far field outer shell, and the trailing-edge plane. The symmetry plane is generated as a single surface, but is actually three sides of the computational space as described in the grid topology section. It is desirable to directly control grid spacing and shape upstream of the root chord, and spanwise beyond the wingtip. To control the wingtip region, the delta wing grid is divided by a 2-D surface grid along the wing trailing edge extending outwards to the far-field grid. Grid spacing on the 2-D divider grid is specified in both spanwise and vertical directions, thus, providing the desired grid control in the wingtip region. The 3-D grid upstream of the wing trailing edge is complex in topology and is created by the 3-D elliptic grid generation program, which, when properly applied, produces a smoothly varying grid. The downstream grid, on the other hand, is essentially 2-D in topology and is created by an algebraic method. The junction between the two subgrids is not continuous in regards to grid line slope, but a mild variation in slope continuity will not produce significant errors in a finite volume flow solver.

TWO-DIMENSIONAL BOUNDARY GRIDS (2-D)

The wing surface topology as previously described, is not unique, but is very demanding of the grid generation method. A desirable feature of such a method is the ability to specify the grid spacing along the root chord, trailing and leading edges, then assimilate this spacing smoothly into the interior of the grid. A method for generating quasi 2-D grids on curved

surfaces by Thomas (Ref. 3) exhibits the desired feature. The quasi 2-D method was derived from the 3-D elliptic grid generation method by Thompson (Ref. 2), by rewriting the 3-D equation for grid points being constrained to a 3-D surface. Thus, the 2-D method accounts for grid point spacing and position based on a 3-D position vector, not a 2-D position vector. The wing leading-edge region is where the added dimension makes the biggest difference. An additional term in the quasi 2-D method, but not found in the 3-D equations, draws grid points toward regions of high curvature, thus, producing a more accurate modeling of the curvature. The grid spacing in the interior of the grid is controlled by the grid point spacing on the boundaries by adding source terms to the elliptic equation. The source term values are computed solely from the boundary grid point spacing and then interpolated into the interior grid. The final product of this method is a grid that has smoothly varying grid point positions and reflects the grid point spacing of the boundaries. Appendix A lists the quasi 2-D elliptic equations.

WING SURFACE

The wing upper and lower surfaces are generated separately and then joined together. Grid point spacing is specified at four points on the wing surfaces, as shown in Fig. 2c with T1, T2, T3, and T4 as input parameters. The root chord is first spline fitted from the input airfoil shape. Grid points are then distributed along the root chord based on arc length, with the leading-edge spacing being T1 percent of the total root chord arc length and the trailing-edge spacing being T2 percent of the total arc length. A hyper-bolic tangent stretching routine, developed by Vinokur (Ref. 4), is used to determine the remaining grid point positions. The grid point spacing along the trailing edge is controlled by the T3 and T4 parameters. The spacing at the wingtip is T3 times T1; therefore, a value of 1.0 for T3 will create an

constant grid spacing along the leading edge over the entire length of the leading edge and wingtip. Even spacing is used along the combined length of the leading edge plus wingtip. The grid spacing along the trailing edge at the root chord is T4 percent of trailing-edge arc length. The remaining trailing-edge points (between T3 and T4) are distributed based on the hyperbolic tangent stretching function.

The wing surface is generated using the quasi 2-D method and the boundary spacing as just described. The thickness of the wing at each grid point is linearly interpolated from airfoil cross sections provided as user input. The wingtip is rounded over the last 2 percent of semispan as seen in Fig. 5.

PLANE OF SYMMETRY

The plane-of-symmetry grid (or wall in a wing-on-a-wall calculation) is created by the same 2-D elliptic method as the wing surface, simply by rotating the symmetry plane into the wing plane and setting all thickness values to zero. The symmetry plane is divided into upper and lower halves, and a separate grid is generated for each half. The two halves are rejoined and the joining line is adjusted to give smooth grid lines across the joint. The upper and lower halves of the symmetry plane with the sides numbered for reference are shown in Fig. 6a-d. Side two is the wing root chord with grid point spacing defined by the wing surface grids. Sides one and four were straight lines with grid spacing at the root chord, far field and overall lengths of these lines specified by the user as input parameters T5, T6, and T7 on side one and T8, T9, and T10 on side four. The remaining grid points along sides one and four are distributed using the hyperbolic tangent stretching routine.

Once the upper and lower halves of the symmetry planes are created, the grid points on side one are adjusted to obtain continuous second derivatives

8

in grid spacing for the family of lines crossing side one. By using two grid points on one side of side one and one grid point of the same curve on the other side, second derivatives in grid spacing can be computed on both sides of side one. By averaging the two values obtained, a first-order accurate approximation of the second derivative in grid spacing is obtained for points on side one. Using this approximation and the position of the grid points immediately on either side of side one, the grid points on side one are repositioned to satisfy the second-order derivative equation written for side one points. The result of this repositioning is a continuous second derivative in grid spacing across the interface of side one.

The 2-D elliptic method used does not directly enforce orthogonality at the boundaries. The S1 term in the source terms influences the curvature of a grid line (Ref. 3 and Appendix A). The source term is normally computed automatically from the boundary grid point position and spacing. By locally adjusting the value of S1, the boundary grids are made more nearly orthogonal. The S1 parameter was set by trial and error, for the grids included in this report at the wing leading edge in the plane-of-symmetry grid, and at the wingtip in the trailing-edge grid to improve orthogonality at the wing surface beyond that which is obtained from using the automatic controls.

TRAILING-EDGE GRID

The 2-D trailing-edge grid divides the total 3-D physical grid into two parts: the portion upstream of the wing trailing edge and the portion downstream of the trailing edge. This grid is created in essentially the same way as the symmetry plane grid, but the trailing-edge shape and thickness is modeled instead of the root chord. The upper and lower halves of the grid are created separately. The halves are joined together and the joint line is then smoothed. Indicated in Fig. 7 is the trailing-edge grid side numbering and

9

spacing parameters used in the computer code. Note the use of T8 and T9 to control spanwise grid spacing.

Side two is the wing's trailing edge and is generated during the wing surface grid calculations. Sides one and four are straight lines with end point grid spacing and overall lengths specified as input parameters. The remaining side one and side four grid points are distributed by the 1-D hyperbolic tangent stretching routine. Side three is elliptic in shape and has even grid point spacing. Figures 8a and b show a typical trailing-edge grid. Even though this grid is generated in 2-D, the wing trailing edge need not be a straight line.

FAR-FIELD CAP GRID

The last grid required to complete the boundaries of the 3-D physical space is the far-field cap grid. This grid is an ellipsoid that is created using the quasi 2-D elliptic method. The far-field cap is identical to the wing surface in topology and side numbering (Figs. 9a and b). All sides except the elliptical shaped side three are defined by sides of the other quasi 2-D surfaces. An even grid spacing for the entire farfield cap is used on side three.

THREE-DIMENSIONAL GRID (3-D)

The 3-D grid method used to generate the delta wing grid was developed by Thomas (Ref. 3). This method is also the basis for the 2-D method previously described. The standard 3-D elliptic equation was extended to Poisson's equation by inclusion of source terms that caused a mimicking of the 2-D boundary grid point spacing in the interior of the 3-D grid. Appendix B outlines the 3-D elliptic equations used in this method. Since all grid spacing control is evaluated from the 2-D boundary grids in this method, the 3-D grid generator can be applied to a variety of topologies without any

10

special considerations. The grid singularity found in this delta wing grid topology did prevent standard calculation of the S1 curvature term at the singularity. The S1 term is not essential to producing a high quality grid and has been included in the 3-D method only for completeness. The second curvature term, S2, is, however, critical to achieving high quality grids around the leading edge of the delta wing. This term is computed automatically from the 2-D boundary grids and then interior values are interpolated from the boundary values.

The method used to determine the values of S1 and S2 in the interior of the 3-D grid is 2-D transfinite interpolation, more correctly known as blended bilinear interpolation. The details of blended bilinear interpolation are included in Appendix C.

The 3-D elliptic equations are solved using a point over-relaxation scheme. Point iteration schemes are typically slower to converge than are line iteration and more complex schemes, but are more robust. The iteration process requires that an initial guess of the grid point locations be made prior to iterating. The favorable characteristics range of point iteration schemes permits the initial guess to be generated by simple and quick methods. The method used to generate the initial guess is blended trilinear interpolation. The details of blended trilinear interpolation are included in Appendix D.

ALGEBRAIC DOWNSTREAM GRID

The grid downstream of the wing's trailing edge is generated algebraically. A 2-D grid of the same outer shape as the wing trailing-edge grid is constructed at the downstream boundary, consisting of concentric ellipses, with the intermost ellipse being a slit line. The spacing of grid points on the slit line and the spacing between the concentric ellipses is determined by

11

the computer code. The interior of the downstream grid is generated by simple linear interpolation between the wing trailing-edge grid and the downstream grid. The streamwise spacing of the interior is determined by the hyperbolic tangent stretching routine. The grid spacing along the K-varying lines is continuous across the wing's trailing edge.

COMPUTER PROGRAMS

Two computer programs perform the grid generation described in this paper. The first program generates the six 2-D sides (a more correct term would be "surfaces") of the 3-D grid as outlined in parts 1-5 of this section. Appendix E provides directions for use of this program. The second program generates the complete 3-D grid and requires only the output of the first program as input data.

\

SECTION IV

GRID APPLICATIONS

The 2-D and 3-D elliptic grid generation codes described in this paper
have been applied to several geometries. Two configurations of interest for
which Euler solutions have been obtained are a cropped delta wing and a blunt
nose missile body. The cropped delta wing configuration is depicted in Figs.
1-9. Euler solutions for this configuration at Mach numbers of 0.4 and 0.85
are in good agreement with experimental results. Drag polars for this
configuration (Figs. 10 and 11) indicate that the generated grid appears
adequate to capture the major flow features, including what appears to be
vortex breakdown. The predicted drag polar has been shifted to reflect zero
lift drag.

The delta wing grid topology was applied to a blunt nose elliptical cross
section missile body (Ref. 5). The missile nose grid and a slice through the
3-D space is shown in Fig. 12, and the 2-D missile base grid (corresponding to
the delta wing's trailing edge) is shown in Fig. 13. Again the 3-D grid
generated appears adequate to resolve the major flow features of this configu-
ration as is demonstrated by the excellent agreement between predicted and
experimental normal force coefficients at Mach 2.0 for angles of attack up to
14.0 degrees (Fig. 14).

SECTION V

CONCLUSIONS

A grid topology and grid generation method for delta and cropped delta wings has been described and demonstrated. The grid topology has been adapted from a similar topology previously used for a different application. The grid generation method uses a blend of partial differential equations and algebraic interpolation. The resulting grids have been used in conjunction with an Euler equation solver to accurately predict the flow about two configurations. The quality of the prediction is extremely comparable to results produced in a similar effort of advanced grid generation and flow solution for a delta wing configuration (Ref. 6).
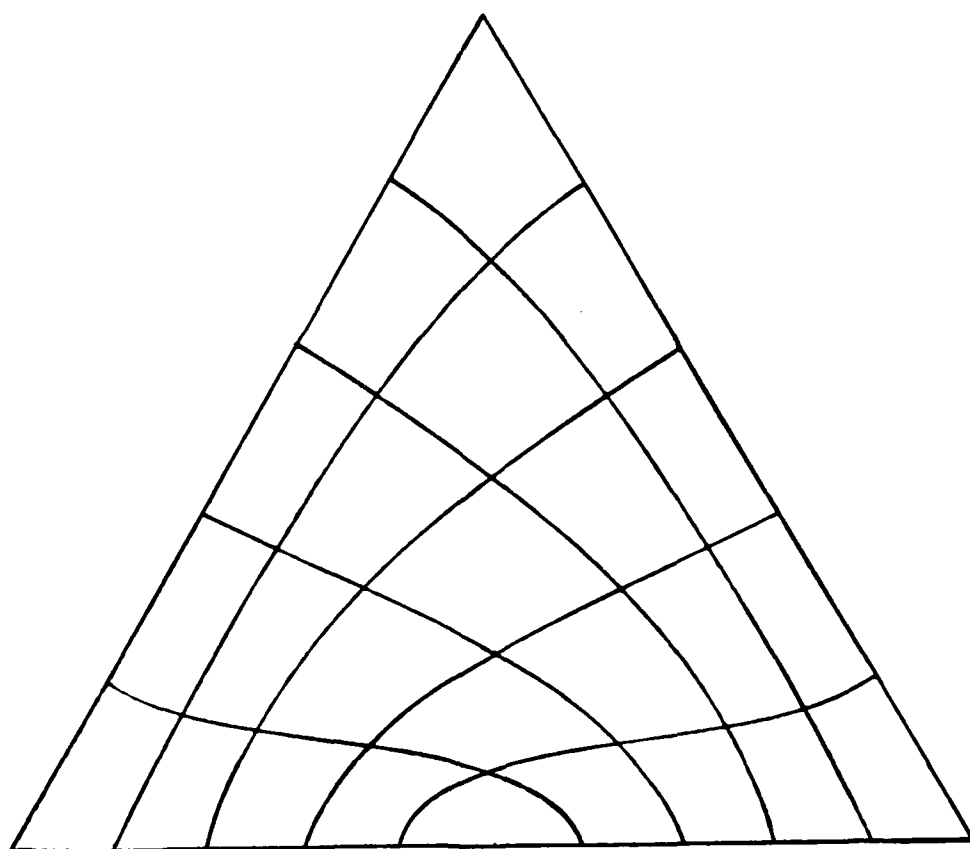
Figure 1. Grid for a Three-Sided Region.

FLOW

SINGULARITY

x

y
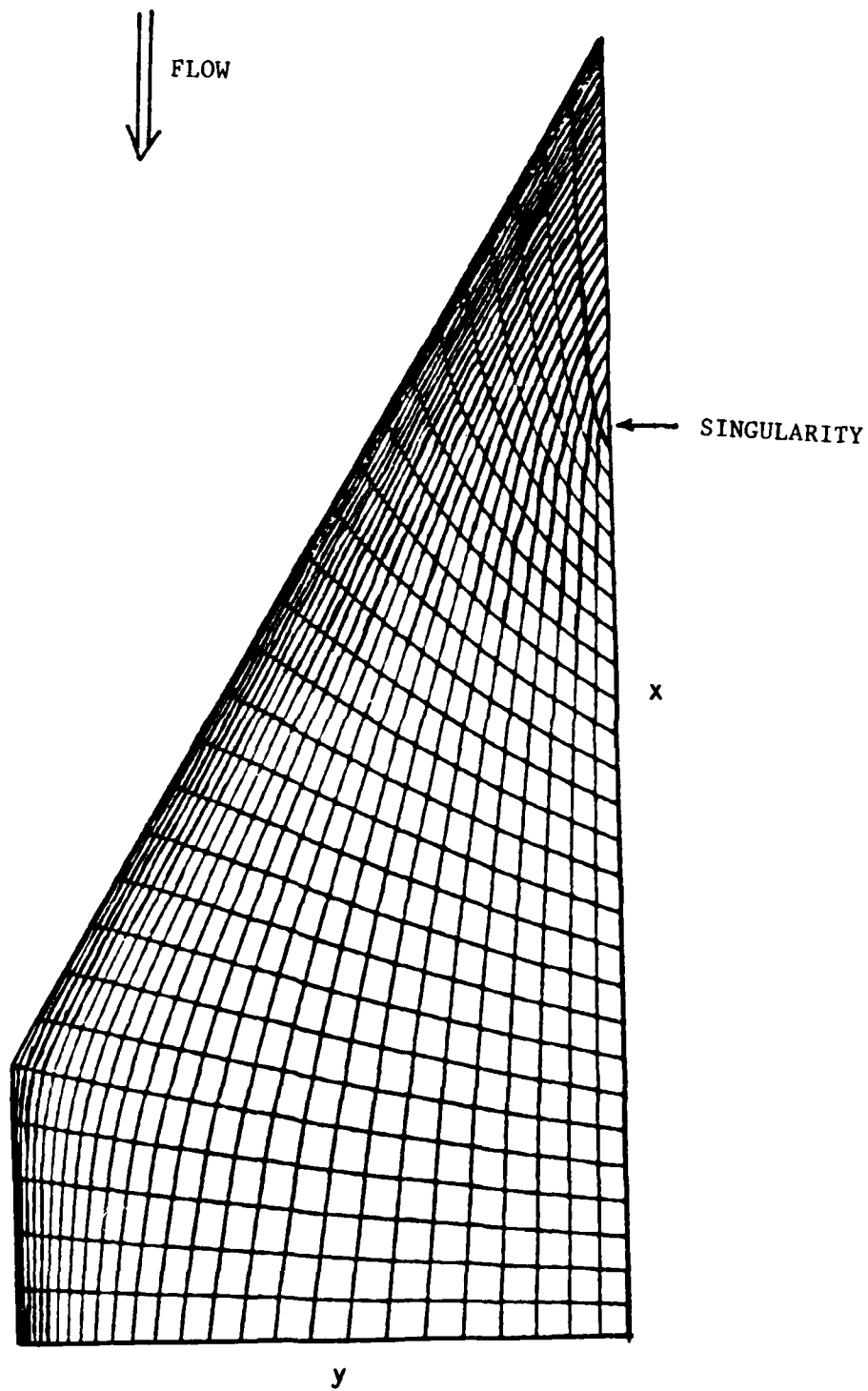
Figure 2a. Delta Wing Surface Grid.

16
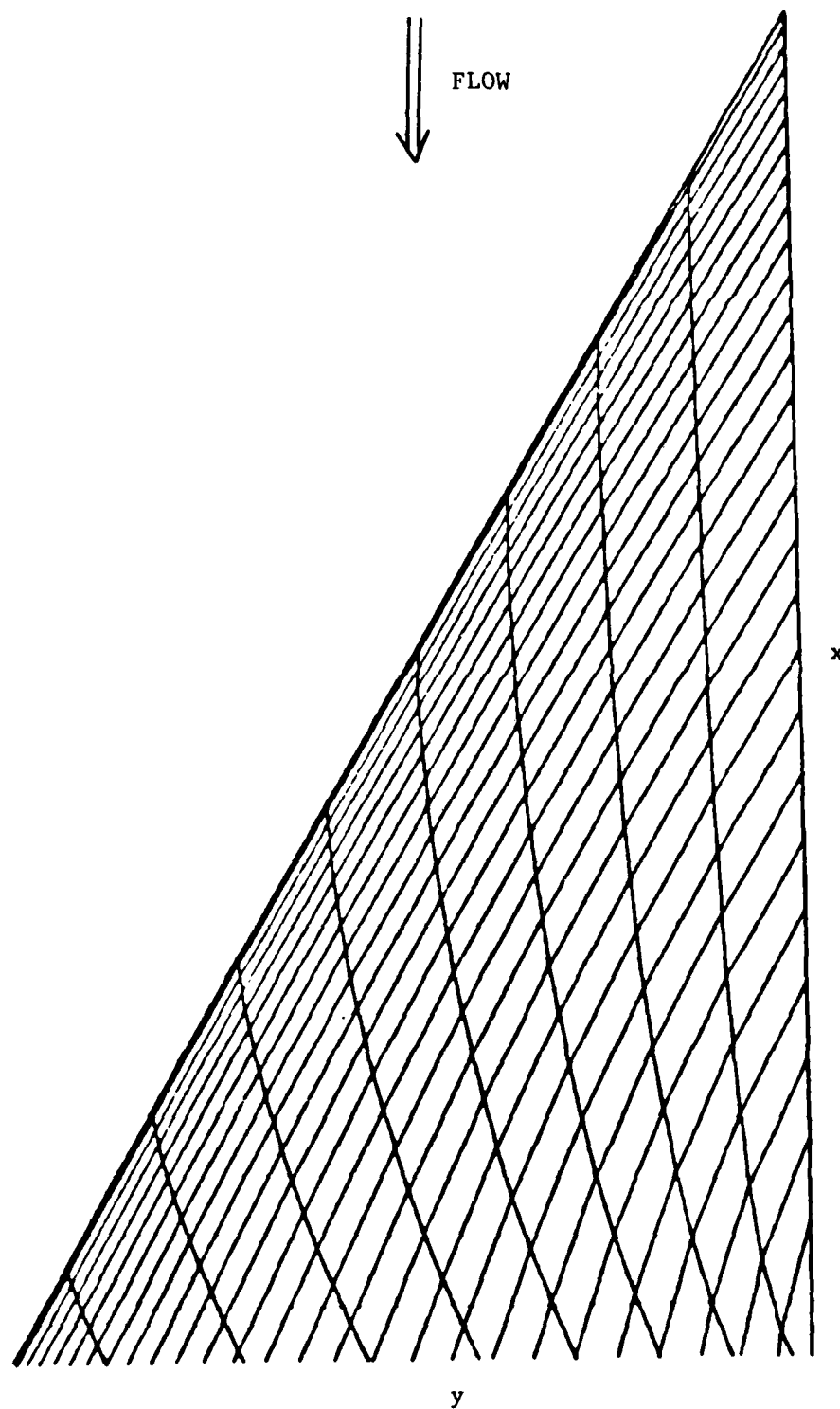
Figure 2b. Detail of Delta Wing Apex.
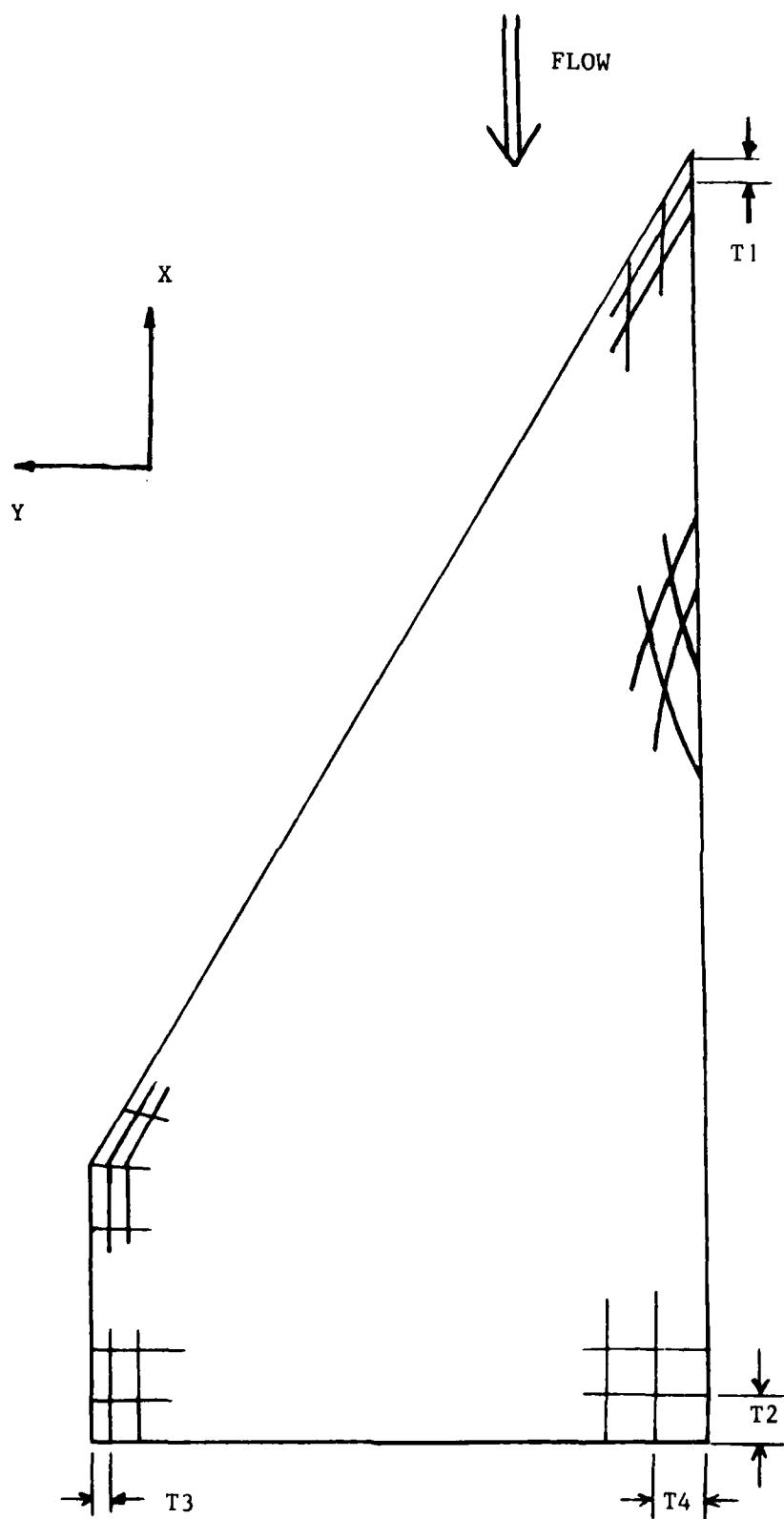
Figure 2c. Wing Surface Grid

18
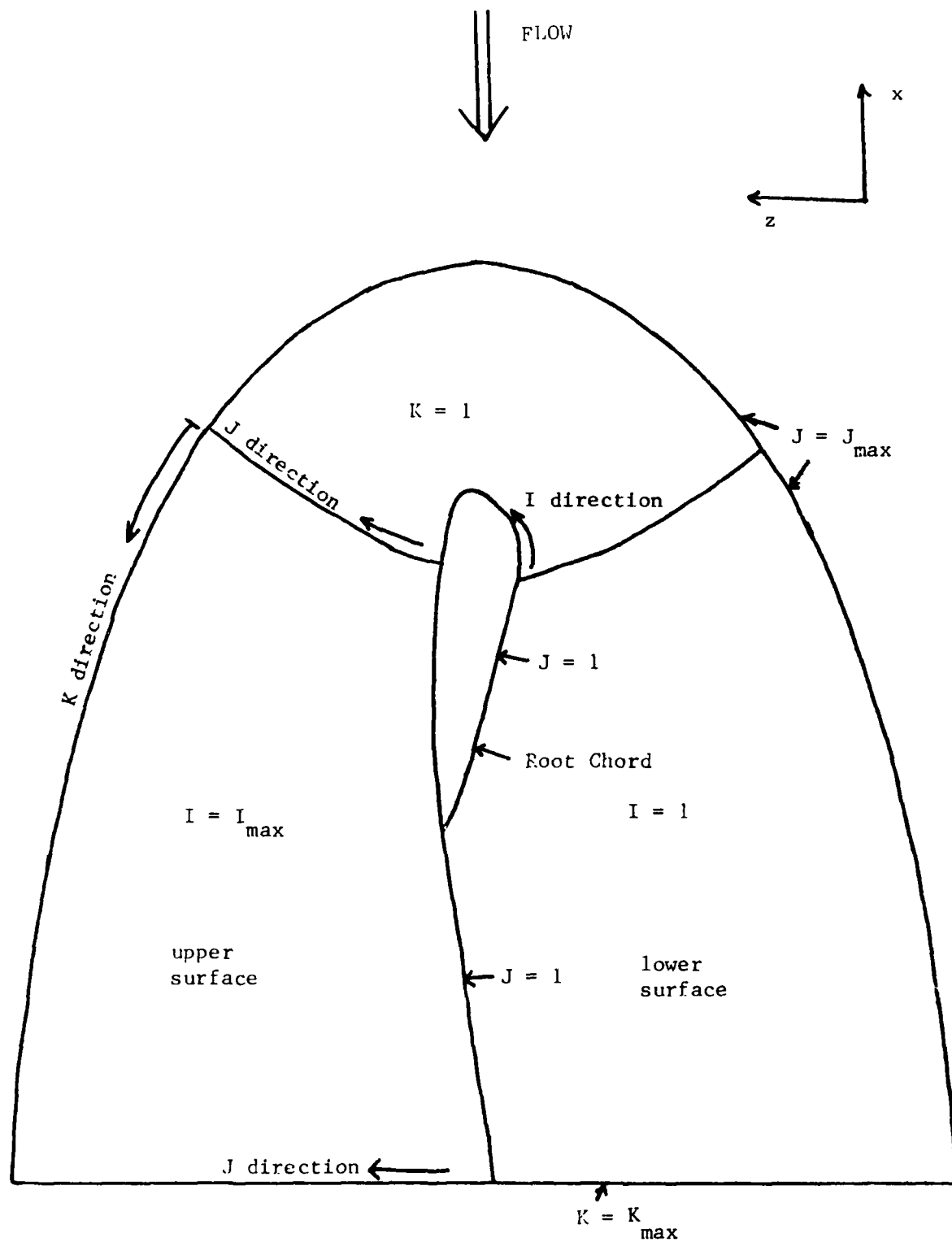
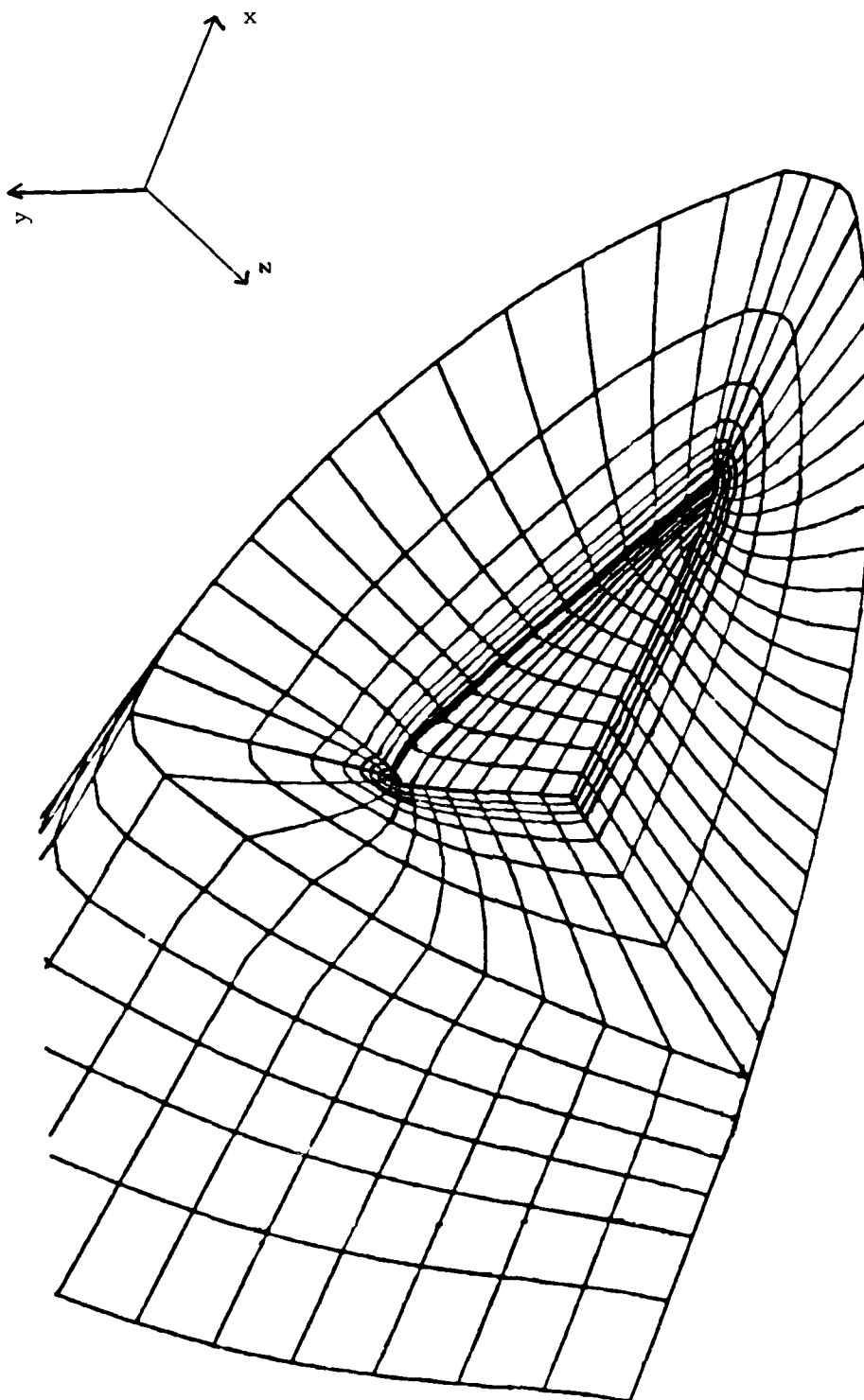Figure 3a. Plane-of-Symmetry Grid Indices
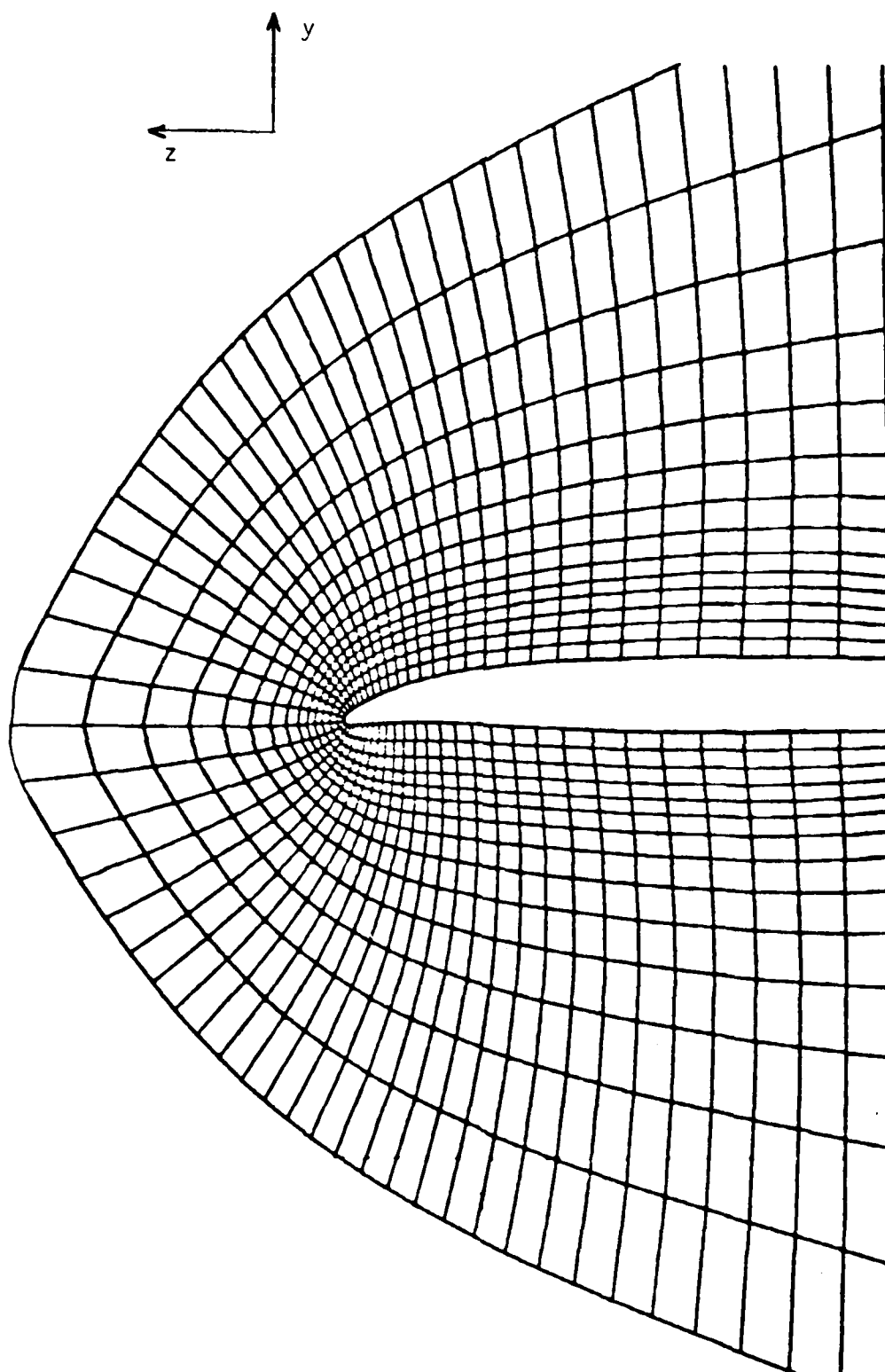
Figure 3b. Cutaway View of 3-D Grid
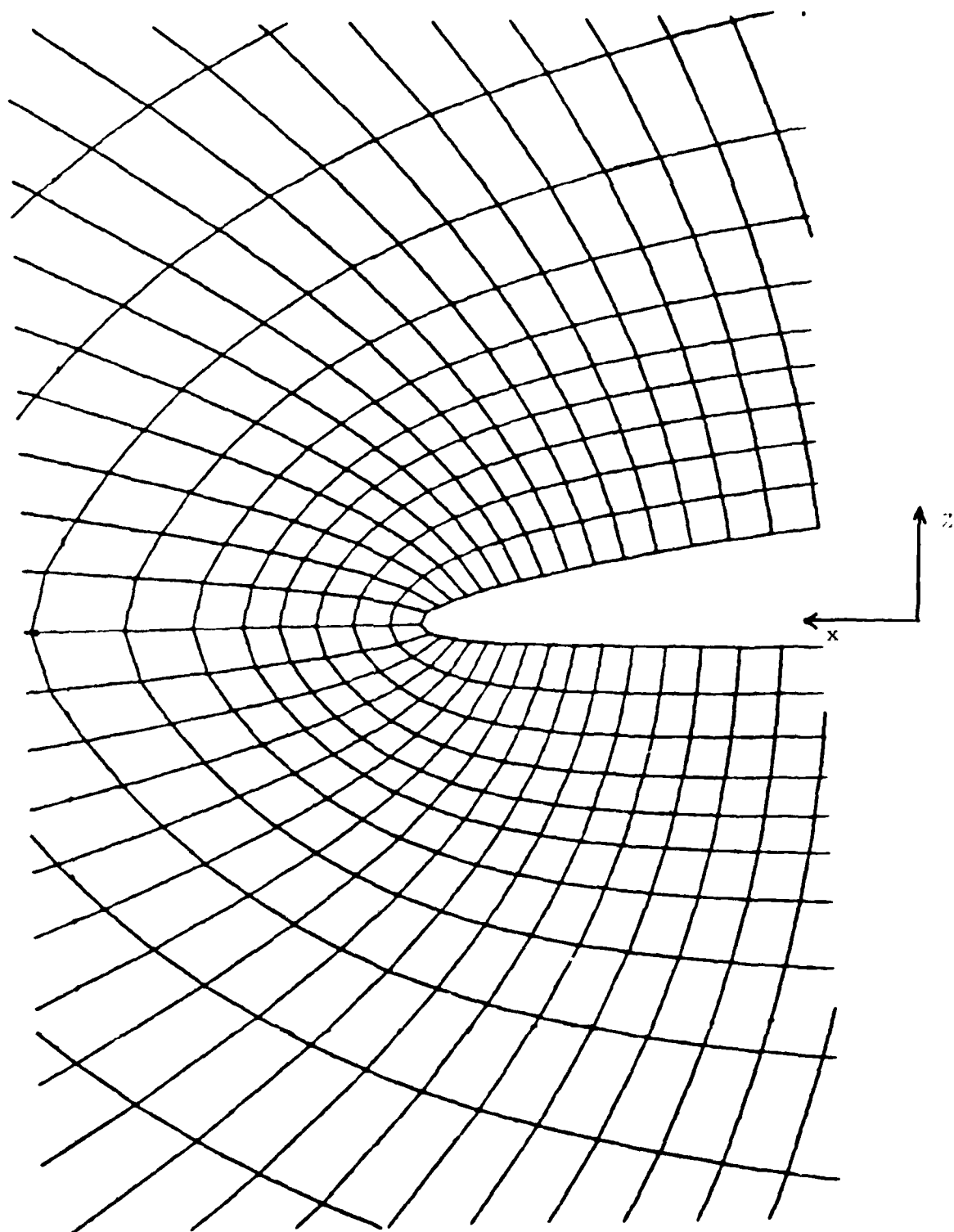
Figure 4a. Typical Spanwise O Grid.
K = Constant Layer

21

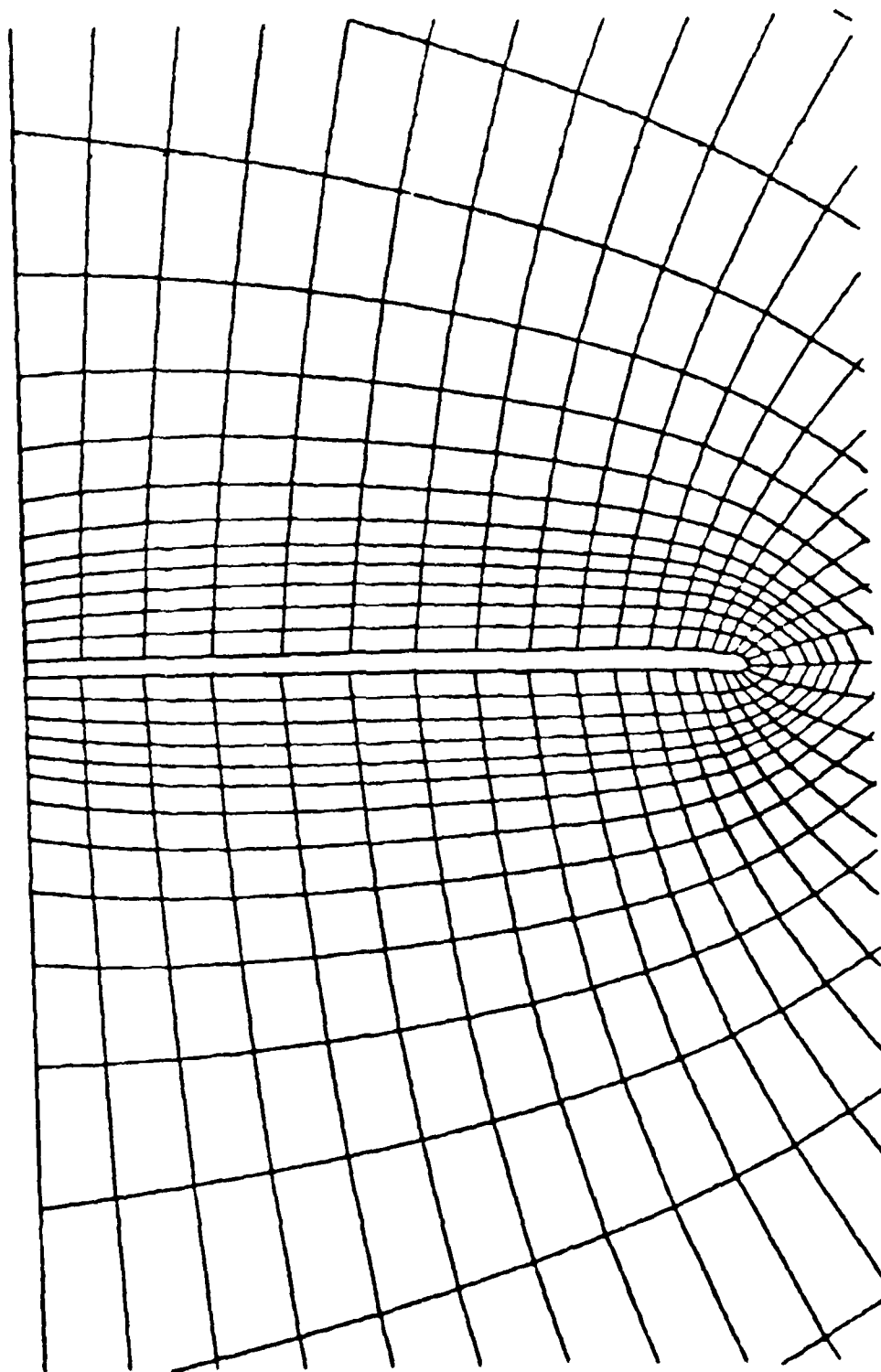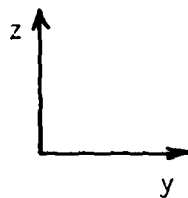Figure 4b. Detail of Leading Edge for a Spanwise O Grid.

22

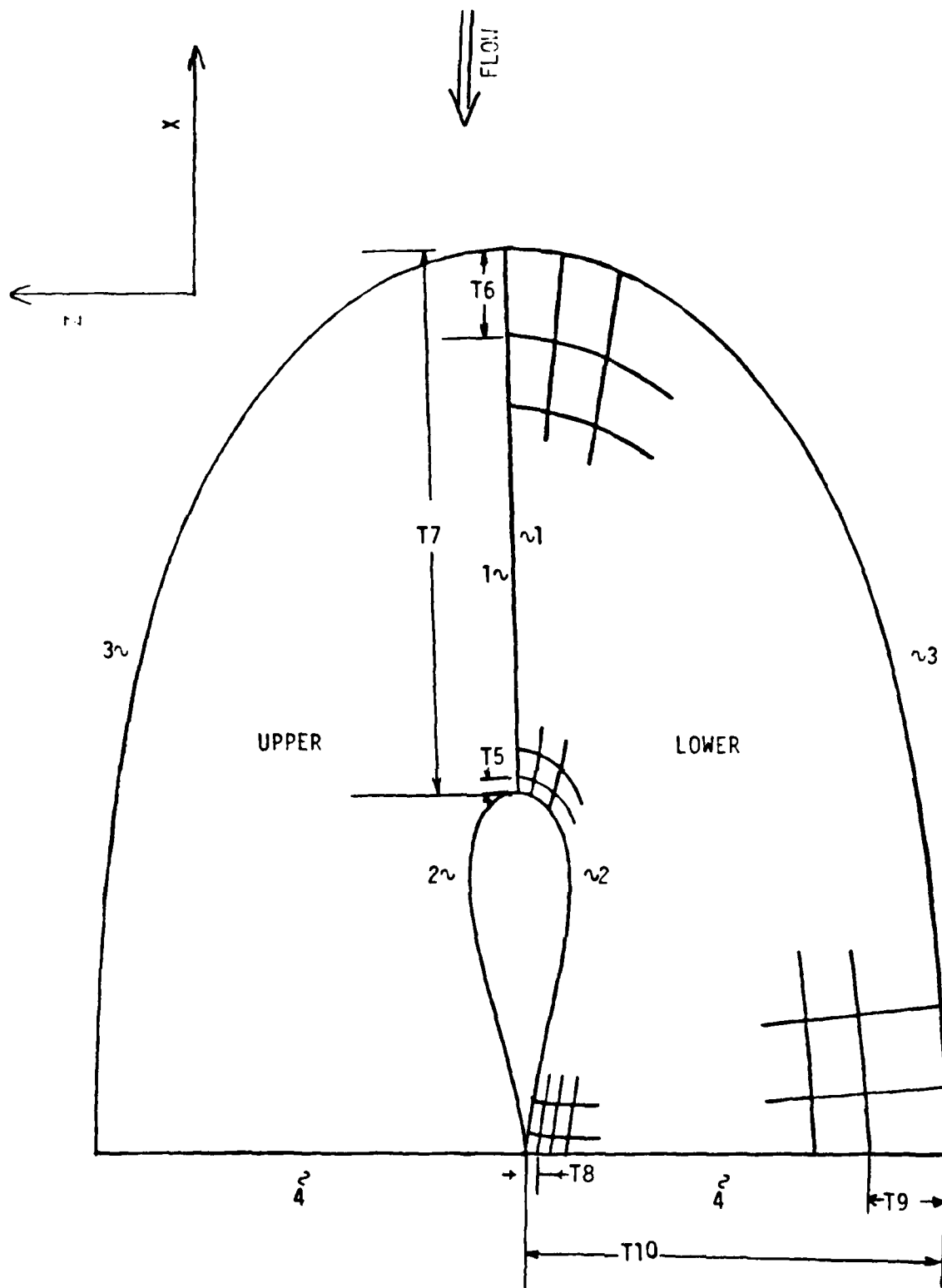Figure 5. K = Constant Grid Layer Showing Rounded Wingtip.

Figure 6a.   Sketch of Upper and Lower Symmetry Plane.
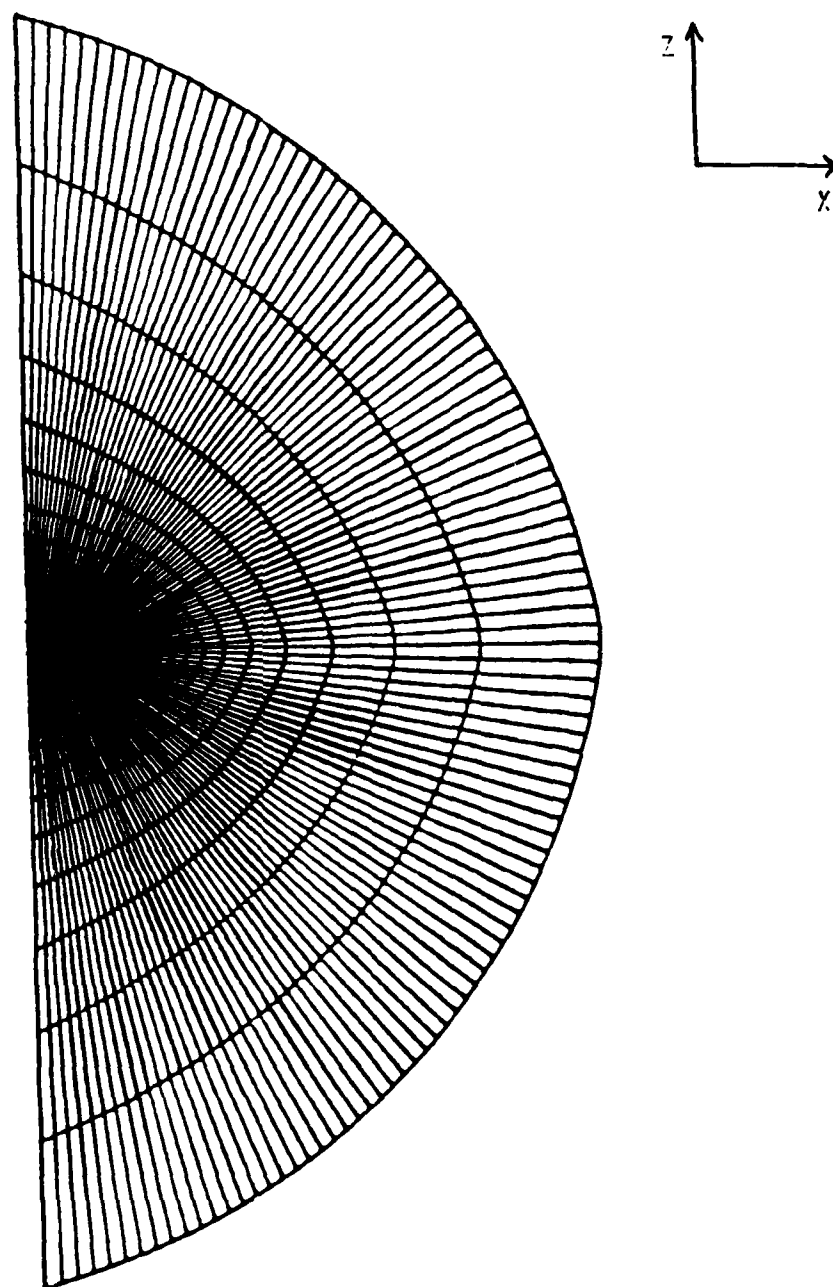
24

Figure 6b. Plane-of-Symmetry Grid.
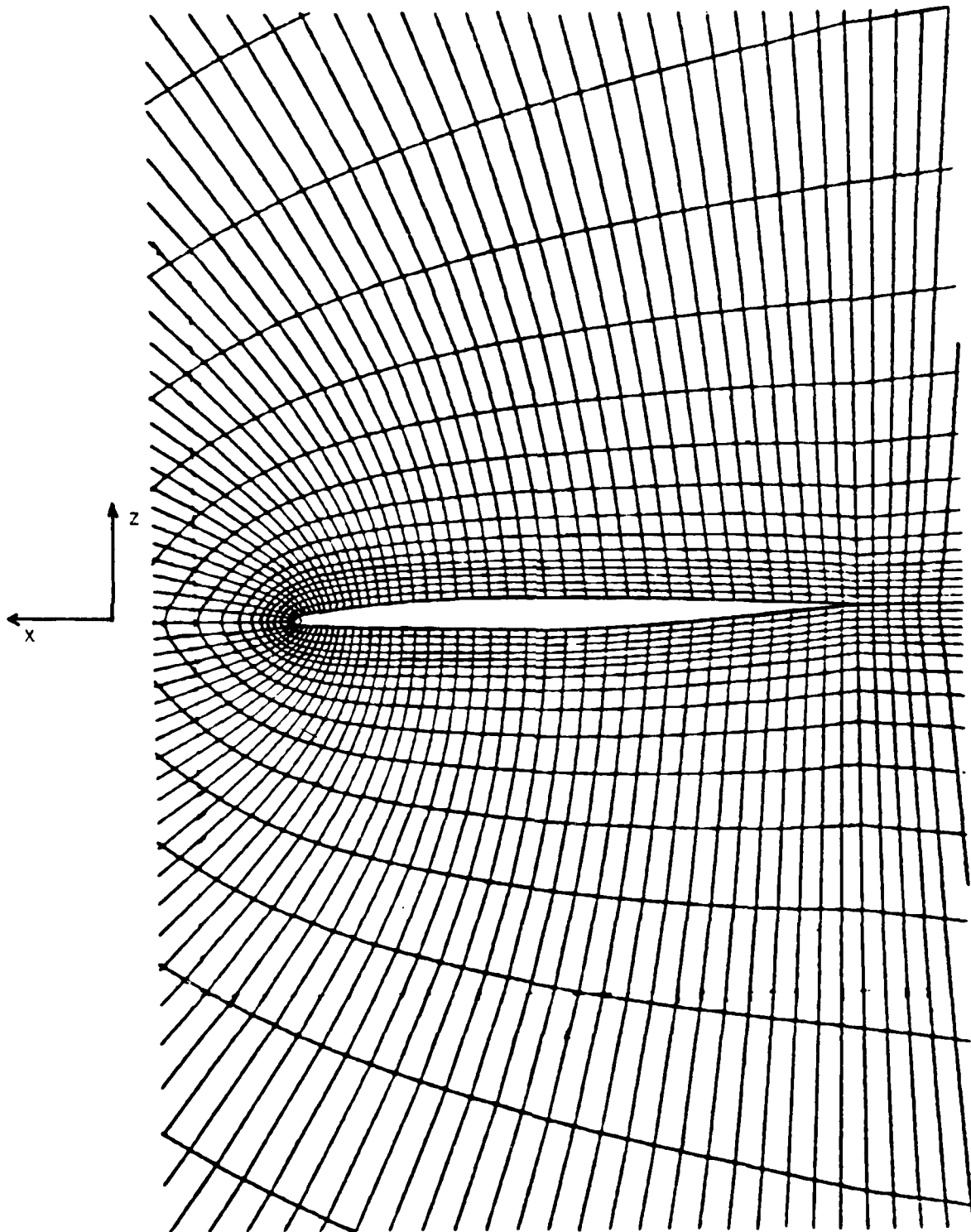
25

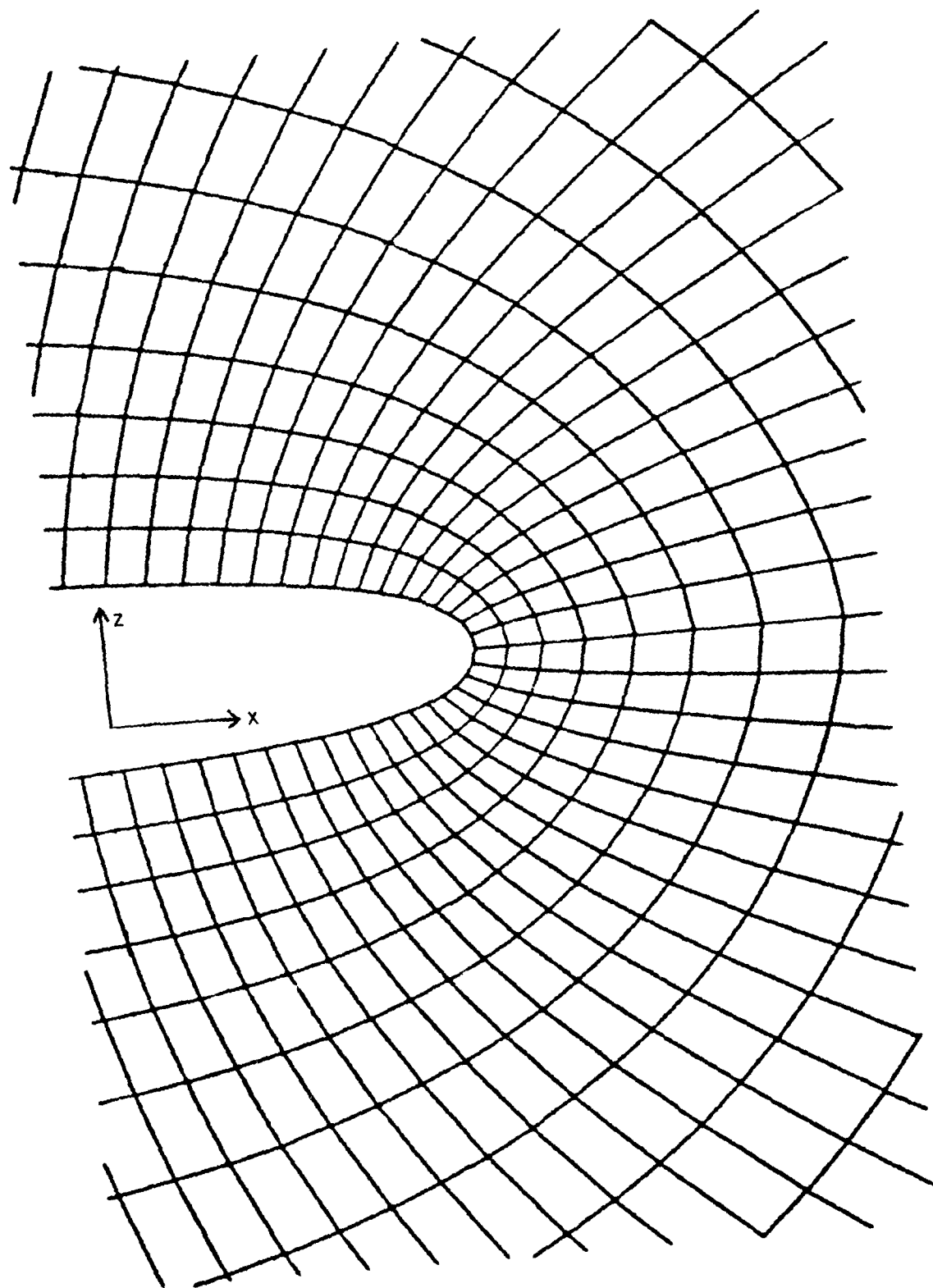Figure 6c. Plane-of-Symmetry Grid Showing Root Chord.

26

Figure 6d. Detail of Root Chord Grid.

27
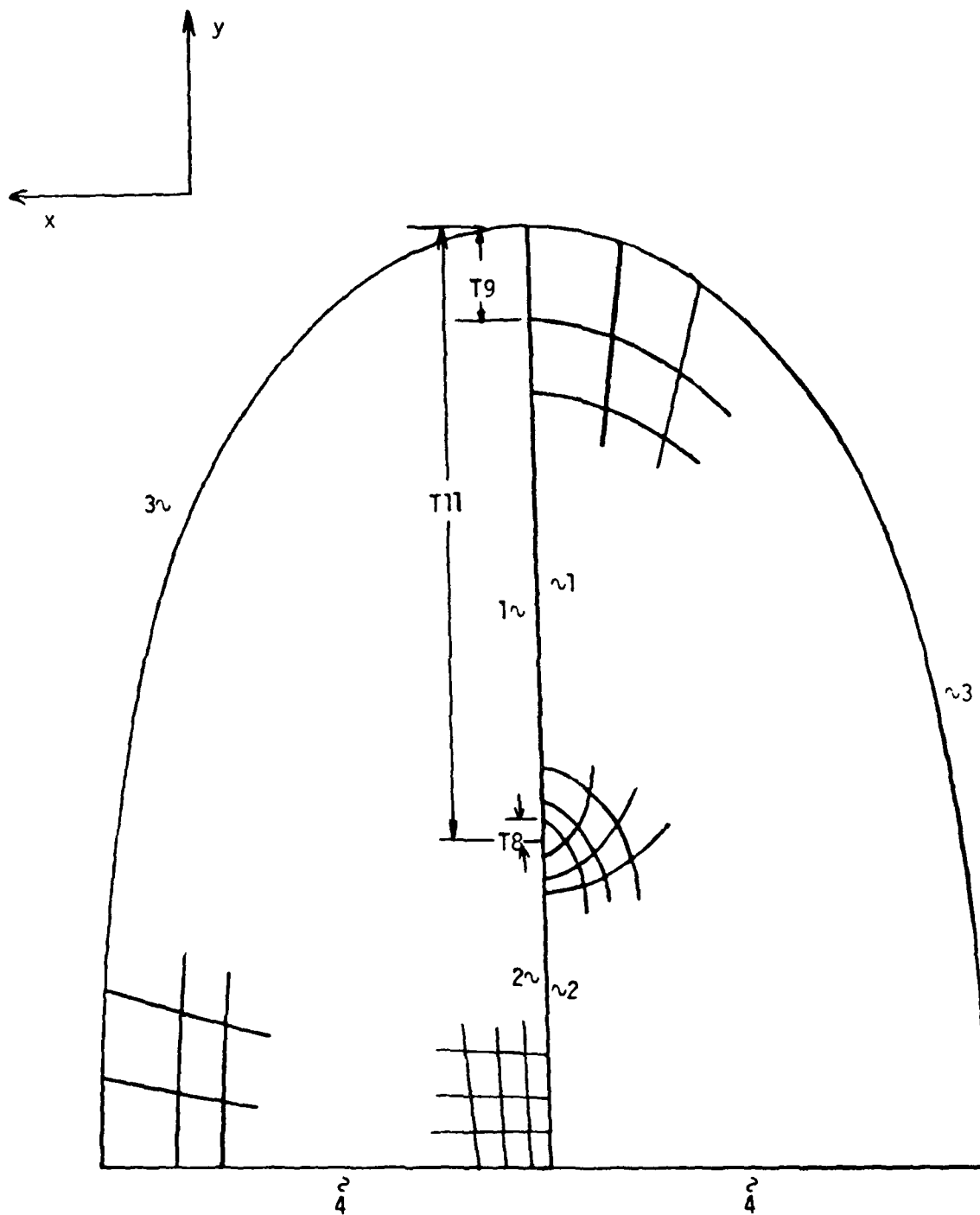
Figure 7. Sketch of Trailing-Edge Grid.
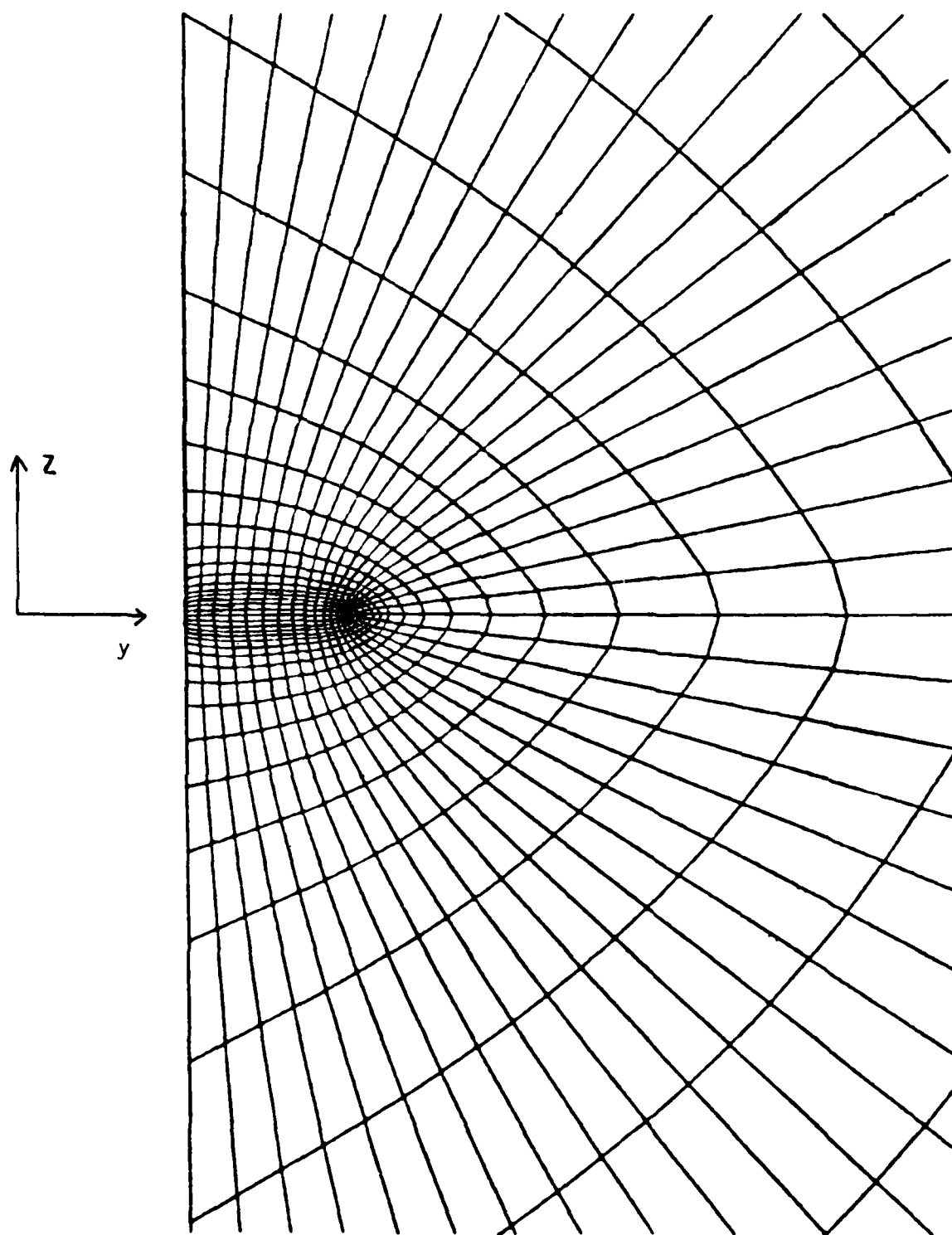
Figure 8a. Trailing-Edge Grid.

29
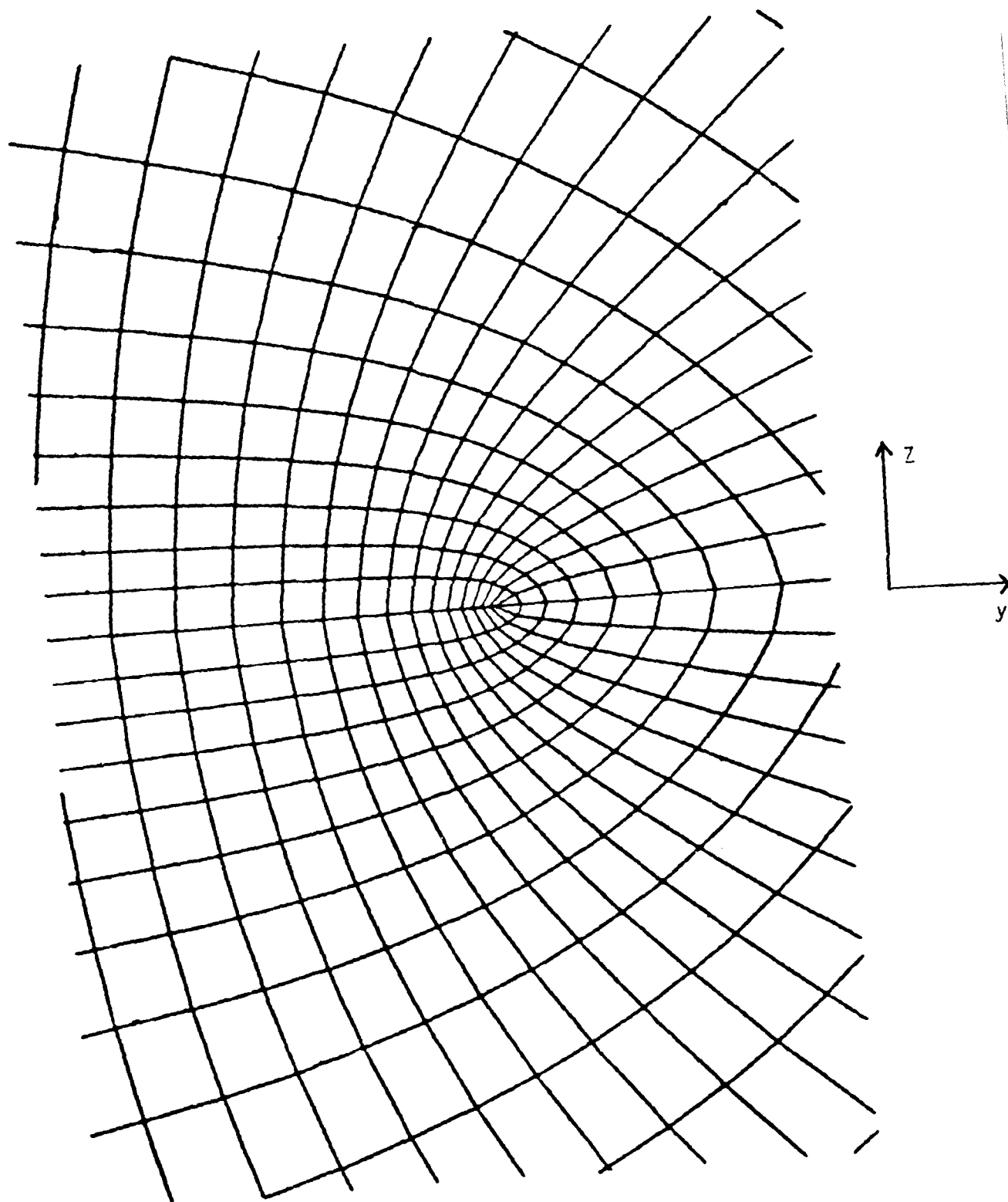
Figure 8b. Detail of Trailing-Edge Wingtip.

30

FLOW

X

y

PLANE OF SYMMETRY

TOP VIEW

Figure 9a.   Sketch of Far-field Cap Grid.

Figure 9b.   Farfield Cap Grid.

32

Figure 10.   Delta Wing Subsonic Drag Polar

Figure 11.   Delta Wing Transonic Drag Polar

33
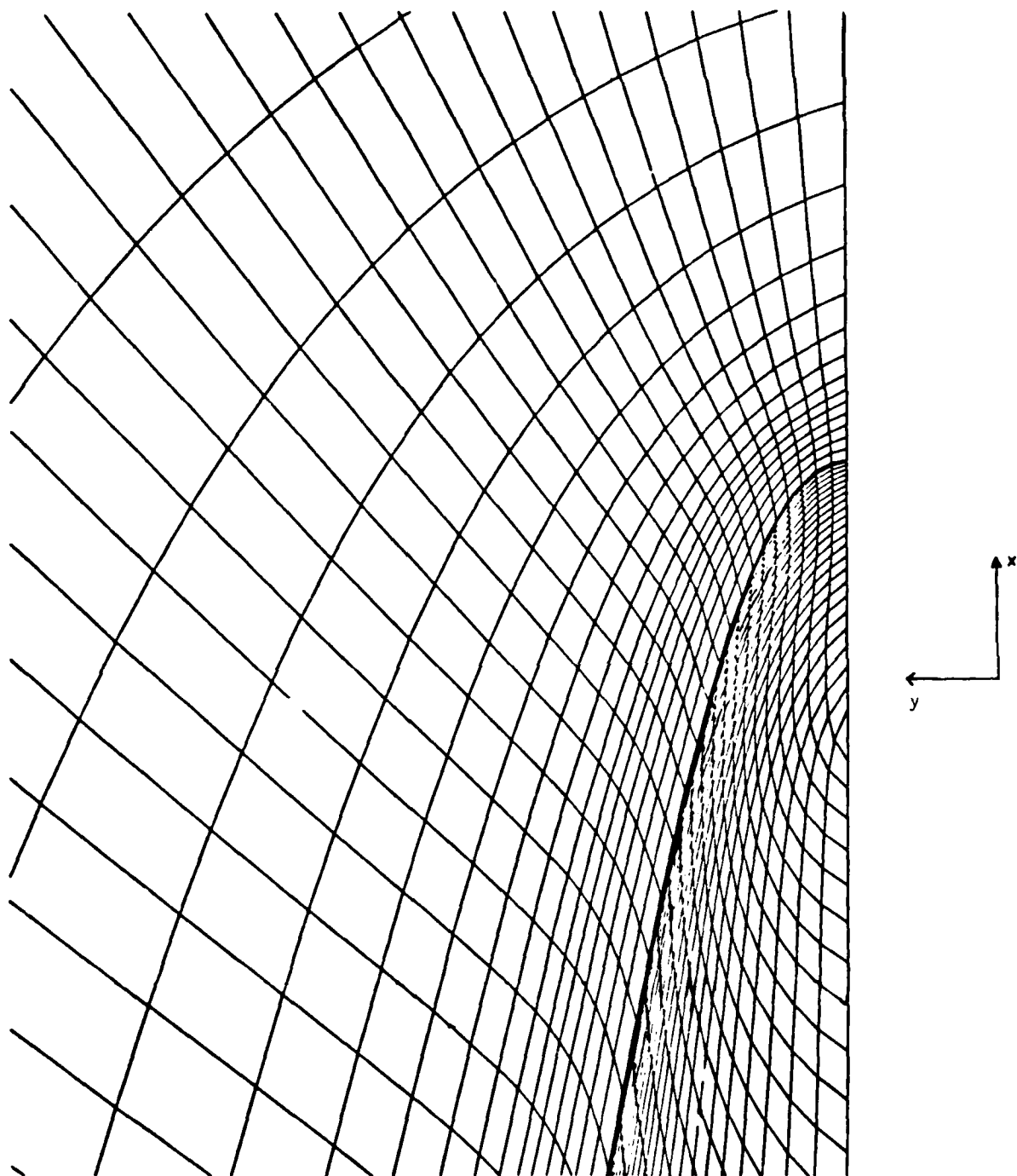
Figure 12.   Elliptic Missile Surface and 3-D Space Grid

34
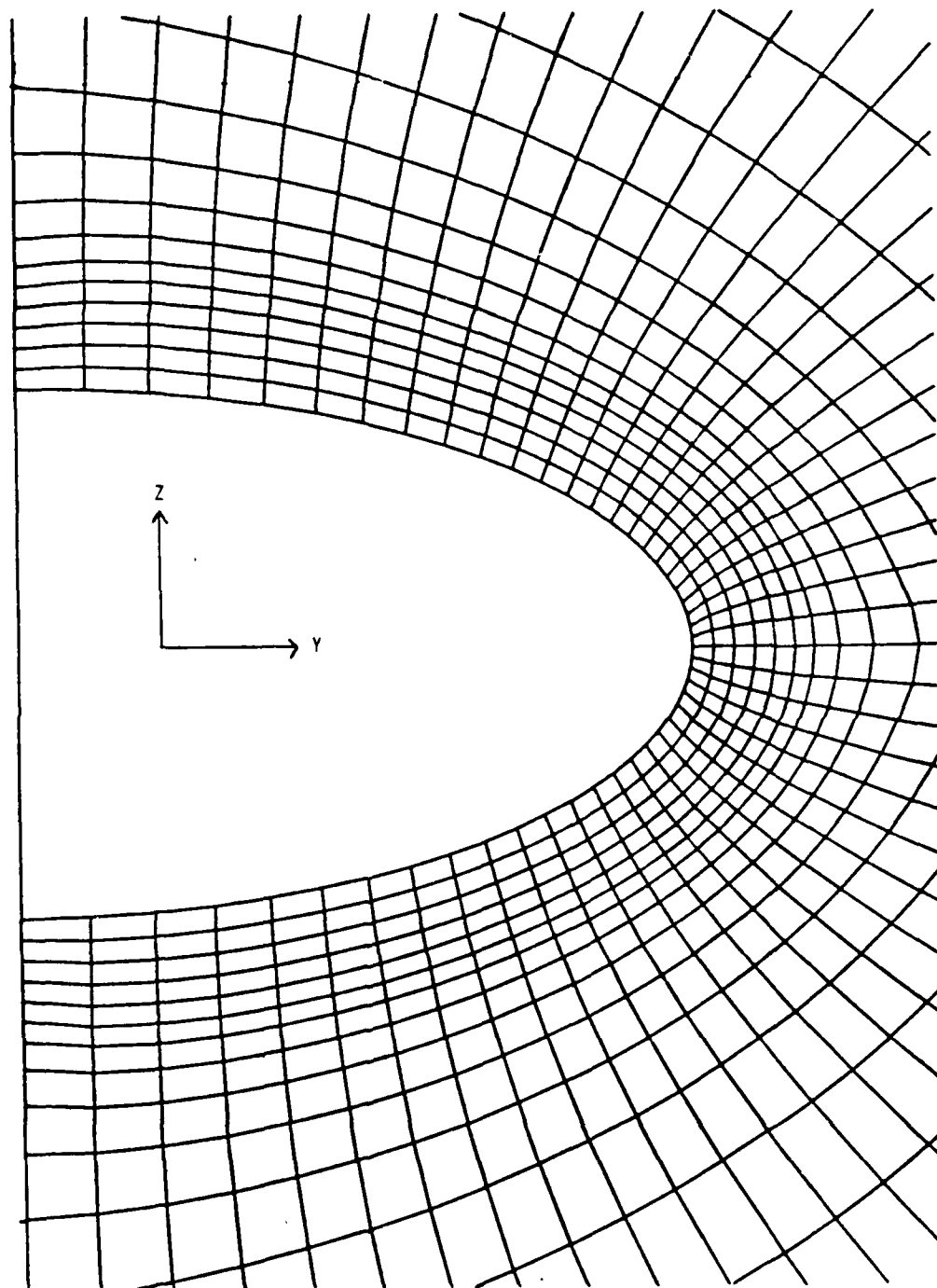
Figure 13. Elliptic Missile Base Grid

35
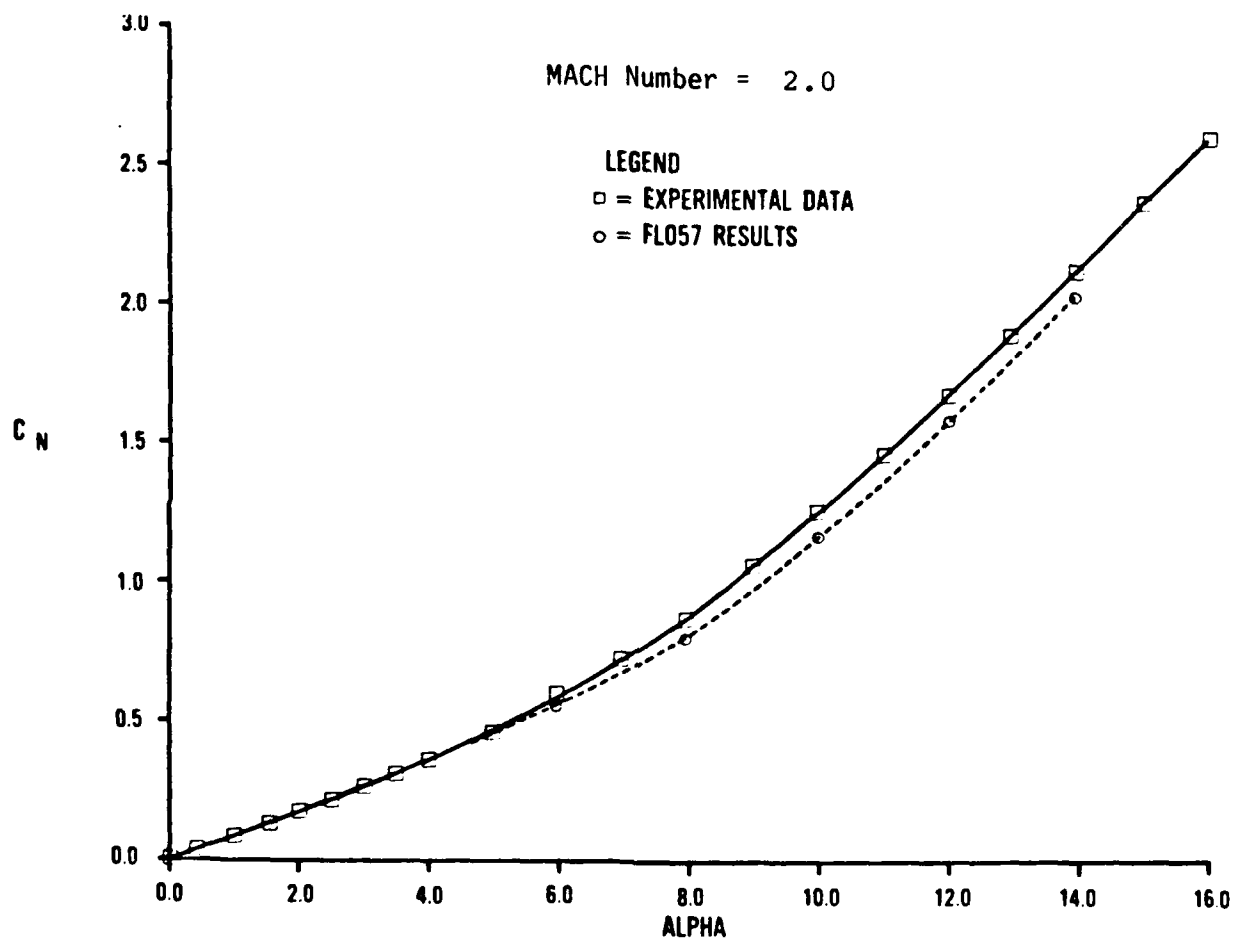
Figure 14. Elliptic Missile Body C_N vs. Alpha

36

REFERENCES

1. Jameson, A., Schmidt, E. and Turkel, E., <u>Numerical Solution of Euler Equations by Finite-Volume Methods Using Runge-Kutta Time-Stepping Scheme</u>, AIAA Paper 81-1259, 1981.
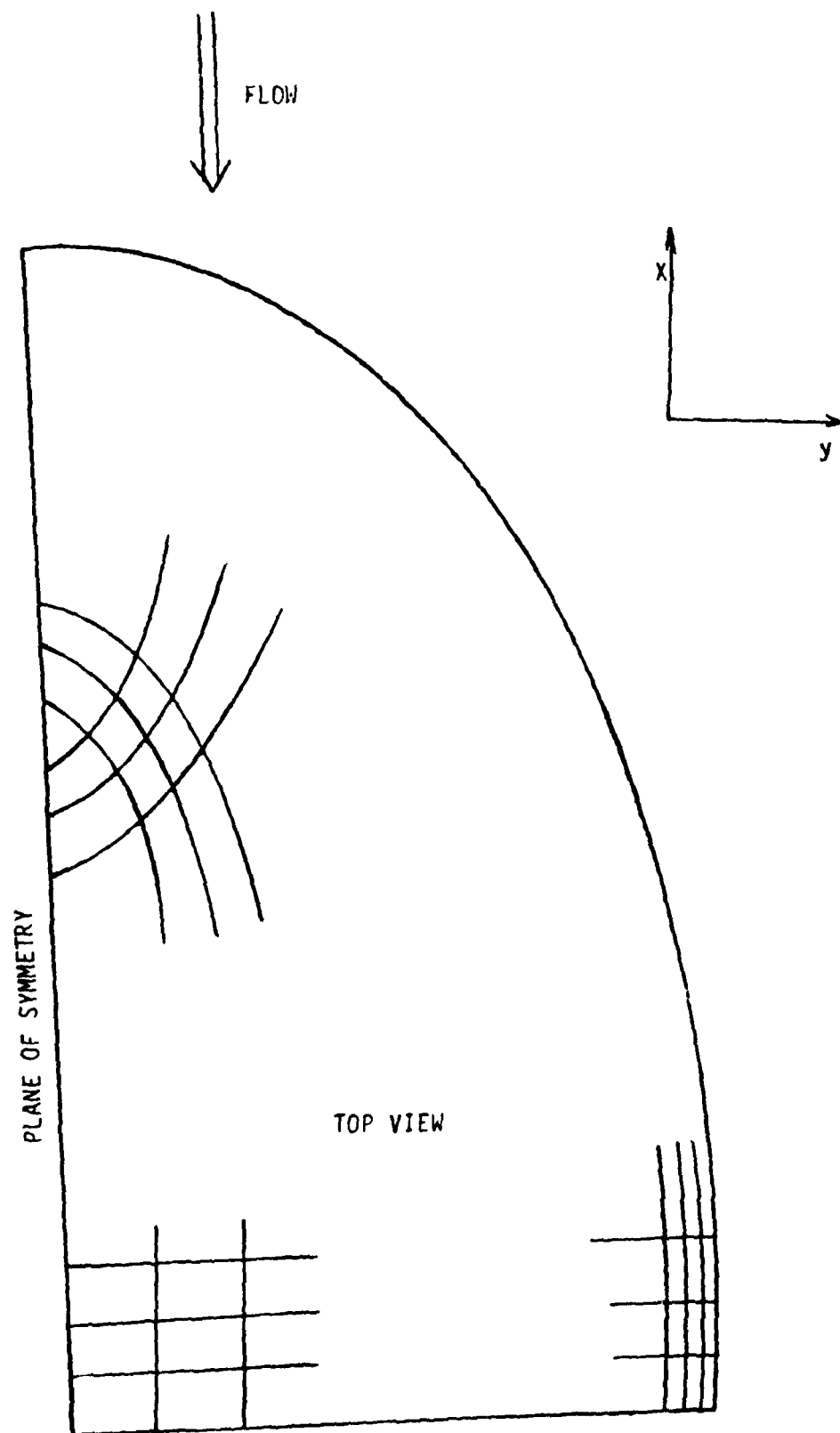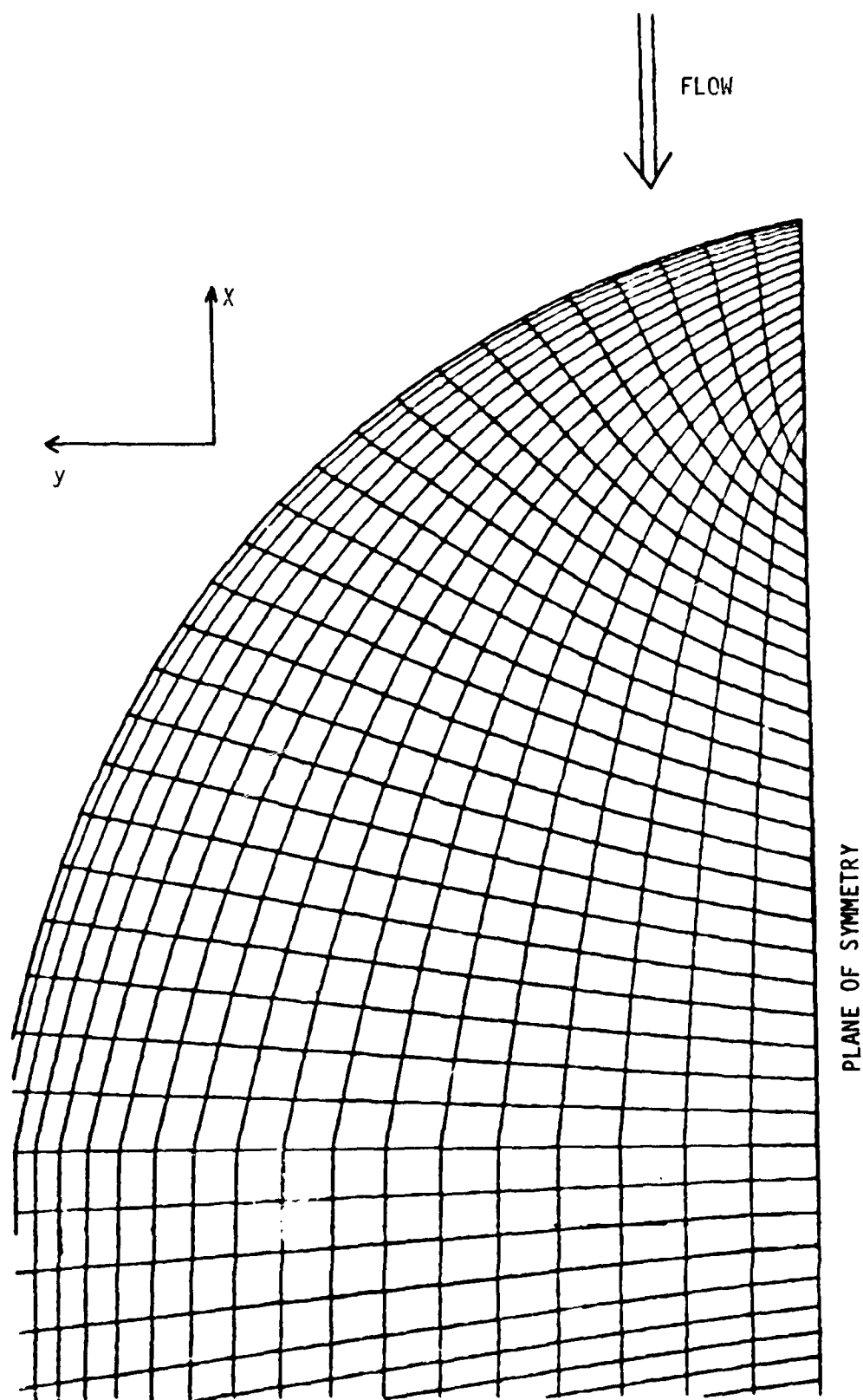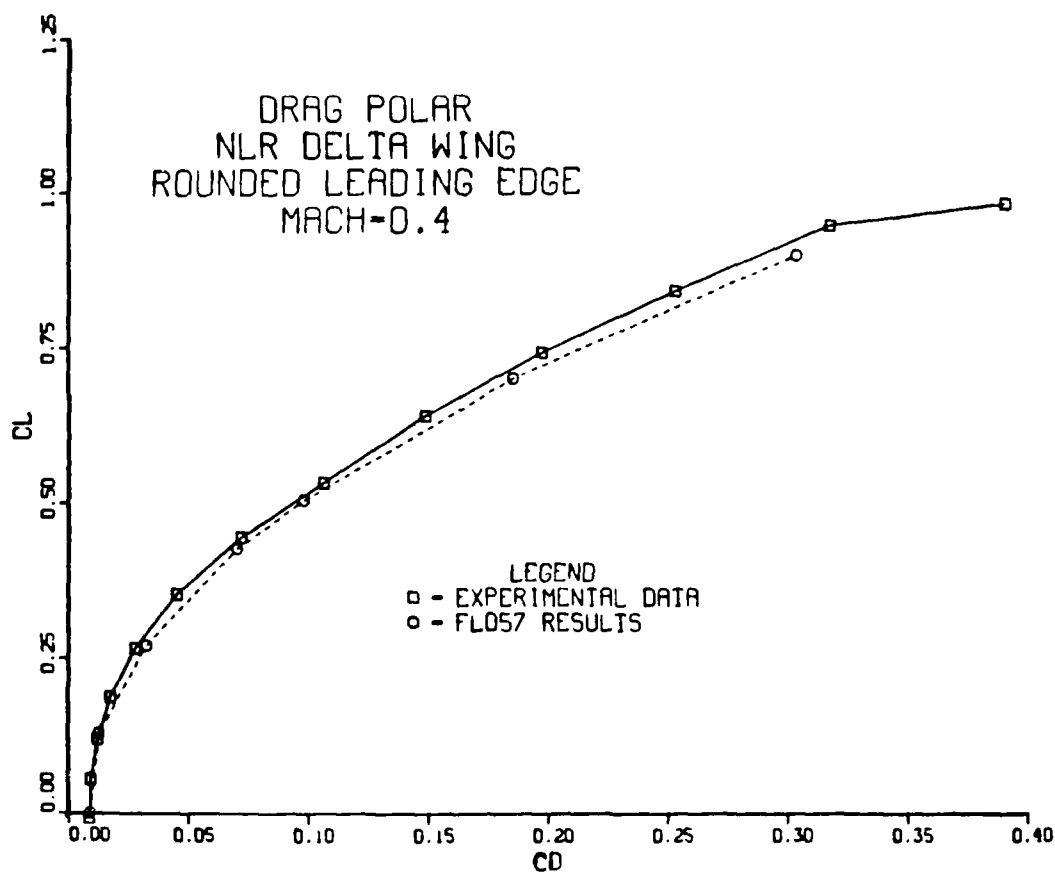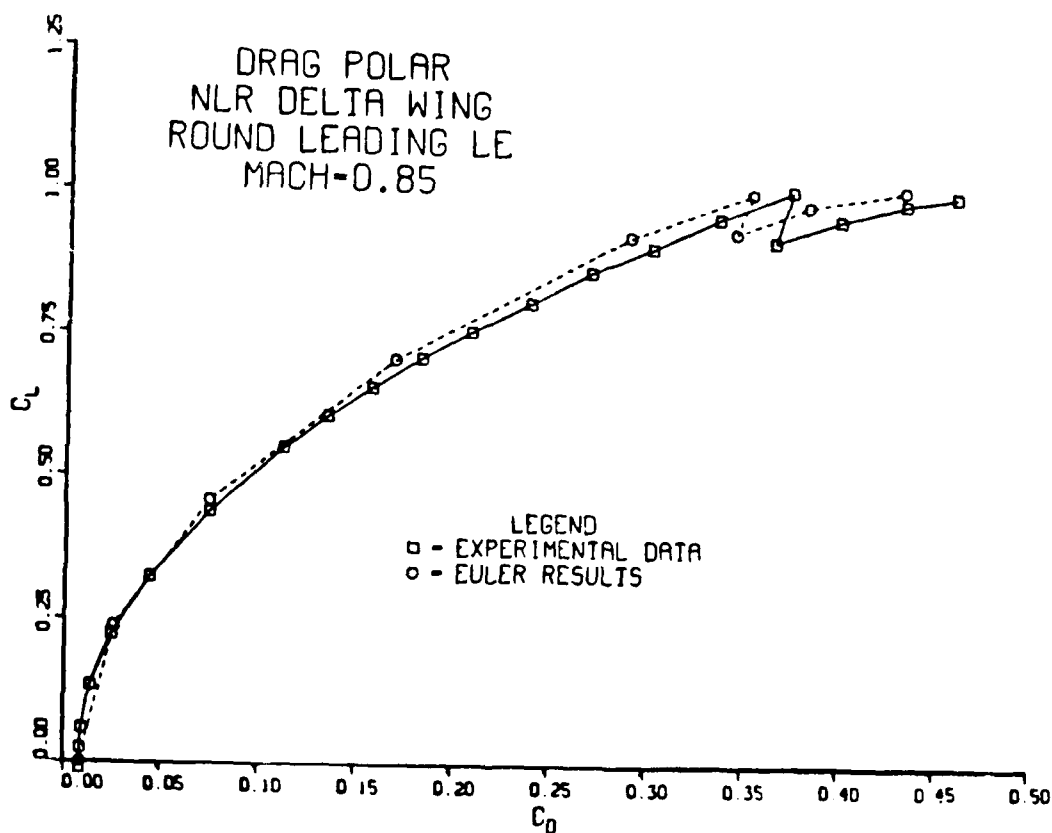
2. Thompson, J.F., Elliptic Grid Generation, pp 79-105 of <u>Numerical Grid Generation</u>, edited by J.F. Thompson, Elsevier Science Publishing Co., Inc., 1982.

3. Thomas, P.D., "Numerical Generation of Composite Three-Dimensional Grids By Quasi-Linear Elliptic Systems," pp 667-686 of <u>Numerical Grid Generation</u>, edited by J. F. Thompson, Elsevier Science Publishing Co., Inc., 1982.

4. Vinokur, M., <u>On One-Dimensional Stretching Function for Finite-Difference Calculations</u>, NASA CR 3313, October 1980.

5. Sirbaugh, J. R., <u>Euler Analysis of an Elliptic Missile Body</u>, AIAA-86-2079-CP, 1986.

6. Fujii, K. and Kutler, P., <u>Numerical Simulation of Leading-Edge Separation Vortex for a Wing and Strake Wing Configuration</u>, AIAA-83-1908, 1983.

7. Gordon, W. and Thiel, L., "Transfinite Mapping and Their Application to Grid Generation," pp 171-192, <u>Numerical Grid Generation</u>, edited by J.F. Thompson, Elsevier Science Publishing Co., Inc., 1982.

37

LIST OF SYMBOLS

2-D	=	two-dimensional
3-D	=	three-dimensional
C_D	=	coefficient of drag, referenced to wing area
C_L	=	coefficient of lift, referenced to wing area
C_N	=	coefficient of normal force, referenced to base area
I, J, K	=	grid indices
I_{max}	=	maximum I grid index
J_{max}	=	maximum J grid index
K_{max}	=	maximum K grid index
S	=	grid generation source term
T	=	grid generation spacing control term

APPENDIX A

QUASI 2-D ELLIPTIC EQUATIONS

(Ref. 3)

$$|r_\eta|^2 (X_{\xi\xi} + \phi X_\xi) - 2 (r_\xi \cdot r_\eta) X_{\xi\eta} + |r_\xi|^2 (X_{\eta\eta} + \psi X_\eta)$$
$$+ f_x G = 0$$

$$|r_\eta|^2 (Y_{\xi\xi} + \phi Y_\xi) - 2 (r_\xi \cdot r_\eta) Y_{\xi\eta} + |r_\xi|^2 (Y_{\eta\eta} + \psi Y_\eta)$$
$$+ f_y G = 0$$

where $r = r (x,y,Z)$, $Z = f (x,y)$

$$G = J_2^2 [(1 + f_y^2) f_{xx} - 2f_x f_y f_{xy} + (1 + f_x^2) f_{yy}]$$
$$/ (1 + f_x^2 + f_y^2)$$

and

$$J_2 = X_\xi Y_\eta - X_\eta Y_\xi$$

$$\phi = - (S_0 + |r_\xi| S_1)$$

$$S_0 = (r_\xi \cdot r_{\xi\xi}) / (|r_\xi|^2)$$

$$S_1 = (r_\xi \cdot r_{\eta\eta}) / (|r_\xi| |r_\eta|^2)$$

$$\psi = - (S_0 + |r_\eta| S_1)$$

$$S_0 = (r_\eta \cdot r_{\eta\eta}) / (|r_\eta|^2)$$

$$S_1 = (r_\eta \cdot r_{\xi\xi}) / (|r_\eta| |r_\xi|^2)$$

Note that S_0 and S_1 for defining ψ are different than S_0 and S_1 for ϕ. For the wing surface $\partial Z/\partial \xi$ was assumed to be zero and the following expressions are used to compute G.

$$f_x = - Z_\eta Y_\xi / J$$

$$f_y = Z_\eta X_\xi / J$$

$$f_{xx} = Z_\eta \eta_{xx} + Z_{\eta\eta} Y_\xi^2 / J^2$$

$$f_{yy} = Z_\eta \eta_{yy} + Z_{\eta\eta} X_\xi^2 / J^2$$

$$f_{xy} = Z\eta \, \eta_{xy} - Z_{\eta\eta} Y_\xi X_\xi / J^2$$

where

$$\eta_{xx} = (-J_\eta Y^2_\xi + JY_\xi Y_{\xi\eta} + J_\xi Y_\xi Y_\eta - JY_{\xi\xi}Y_\eta) / J^3$$

$$\eta_{yy} = (-J_\eta X^2_\xi + JX_\xi X_{\xi\eta} + J_\xi X_\xi X_\eta - JX_{\xi\xi}X_\eta) / J^3$$

$$\eta_{xy} = (J_\eta X_\xi Y_\xi - JX_{\xi\eta} Y_\xi - J_\xi X_\xi Y_\eta + JX_{\xi\xi}Y_\eta) / J^3$$

and

$$J = X_\xi Y_\eta - X_\eta Y_\xi$$

$$J_\xi = X_{\xi\xi}Y_\eta + X_\xi Y_{\xi\eta} - X_{\xi\eta}Y_\xi - X_\eta Y_{\xi\xi}$$

$$J_\eta = X_{\xi\eta}Y_\eta + X_\xi Y_{\eta\eta} - X_{\eta\eta}Y_\xi - X_\eta Y_{\xi\eta}$$

40

3-D ELLIPTIC EQUATIONS

(Ref. 3)

$$\alpha_1 \left(r_{\xi\xi} + \phi r_\xi \right) + \alpha_2 \left(r_{\eta\eta} + \psi r_\eta \right) + \alpha_3 \left(r_{\zeta\zeta} + \omega r_\zeta \right)$$

$$+2 \left(\beta_1 r_{\xi\eta} + \beta_2 r_{\eta\zeta} + \beta_3 r_{\zeta\xi} \right) = 0$$

where $r = (x,y,z)$

$$\alpha_1 = (|r_\eta| \, |r_\zeta|)^2 - (r_\eta \cdot r_\zeta)^2$$

$$\alpha_2 = (|r_\zeta| \, |r_\xi|)^2 - (r_\zeta \cdot r_\xi)^2$$

$$\alpha_3 = (|r_\xi| \, |r_\eta|)^2 - (r_\xi \cdot r_\eta)^2$$

$$\beta_1 = (r_\eta \cdot r_\zeta)(r_\zeta \cdot r_\xi) - (r_\xi \cdot r_\eta) |r_\zeta|^2$$

$$\beta_2 = (r_\zeta \cdot r_\xi)(r_\xi \cdot r_\eta) - (r_\eta \cdot r_\zeta) |r_\xi|^2$$

$$\beta_3 = (r_\xi \cdot r_\eta)(r_\eta \cdot r_\zeta) - (r_\zeta \cdot r_\xi) |r_\eta|^2$$

$$\phi = - S_0 - |r_\xi| \, (T_1 + T_2)$$

$$S_0 = (r_\xi \cdot r_{\xi\xi}) \, |r_\xi|^2$$

$$S_1 = (r_\xi \cdot r_{\eta\eta}) \, / \, |r_\xi| \, |r_\eta|^2$$

$$S_2 = (r_\xi \cdot r_{\zeta\zeta}) \, / \, |r_\xi| \, |r_\zeta|^2$$

$$\psi = - S_0 = |r_\eta| \, (T_1 + T_2)$$

$$S_0 = (r_\eta \cdot r_{\eta\eta}) \, / \, |r_\eta|^2$$

$$S_1 = (r_\eta \cdot r_{\xi\xi}) \, / \, |r_\eta| \, |r_\xi|^2$$

$$S_2 = (r_\eta \cdot r_{\zeta\zeta}) \, / \, |r_\eta| \, |r_\zeta|^2$$

$$\omega = - S_0 - |r_\zeta| \, (T_1 + T_2)$$

$$S_0 = (r_\zeta \cdot r_{\zeta\zeta}) \, / \, |r_\zeta|^2$$

$$S_1 = (r_\zeta \cdot r_{\xi\xi}) \, / \, |r_\zeta| \, |r_\xi|^2$$

$$S_2 = (r_\zeta \cdot r_{\eta\eta}) \, / \, |r_\zeta| \, |r_\eta|^2$$

where the S_0, S_1, S_2 values are redefined for each variable ϕ, ψ, ω.

BLENDED BILINEAR INTERPOLATION

(Ref. 7)

Purpose:

Interpolate function F(s,t) which is known on the boundaries of a 2-D computational space. The computational space has dimension which vary in a direction s from 0 to 1 and in a direction t from 0 to 1.

Assume blended bilinear interpolants of the form:

$$P_s = (1 - s) F(0,t) + sF(1,t)$$
$$P_t = (1 - t) F(s,0) + tF(s,1).$$

The function F(s,t) is interpolated on the computational space by the rule:

$$F(s,t) = P_s + P_t - P_s P_t,$$

or

$$
\begin{aligned}
F(s,t) = \ & (1 - s) && * F(0,t) \\
+ \ & (\quad s) && * F(1,t) \\
+ \ & (1 - t) && * F(s,0) \\
+ \ & (\quad t) && * F(s,1) \\
- \ & (1 - s) * (1 - t) * F(0,0) \\
- \ & (1 - s) * (\quad t) * F(0,1) \\
- \ & (\quad s) * (1 - t) * F(1,0) \\
- \ & (\quad s) * (\quad t) * F(1,1).
\end{aligned}
$$

Grid generation is actually performed on a computational space that varies in an I direction from 1 to I_{max} and in a J direction from 1 to J_{max}. The I and J indices are related to s and t by

$$s = (I - 1) / (I_{max} - 1) \qquad \text{and}$$
$$t = (J - 1) / (J_{max} - 1).$$

43

APPENDIX D

BLENDED TRILINEAR INTERPOLATIONS

(Ref. 7)

Purpose:

Interpolate function $F(s,t,u)$ which is known on the boundaries of a 3-D computational space. The computational space has dimensions which vary in a direction s from 0 to 1, in a direction t from 0 to 1 and in a direction u from 0 to 1.

Assume blended trilinear interpolants of the form:

$$P_s = (1 - s) F(0,t,u) + sF(1,t,u)$$

$$P_t = (1 - t) F(s,0,u) + tF(s,1,u)$$

$$P_u = (1 - u) F(s,t,0) + uF(s,t,1).$$

The function $F(s,t,u)$ is interpolated on the computational space by the rule:

$$F(s,t,u) = P_s + P_t + P_u - P_s P_t - P_t P_u - P_u P_s + P_s P_t P_u$$

where,

$$
\begin{aligned}
P_s P_t = \ &(1 - s)(1 - t) F(0,0,u) \\
+ \ &(1 - s)(\quad t) F(0,1,u) \\
+ \ &(\quad s)(1 - t) F(1,0,u) \\
+ \ &(\quad s)(\quad t) F(1,1,u)
\end{aligned}
$$

$$
\begin{aligned}
P_t P_u = \ &(1 - t)(1 - u) F(s,0,0) \\
+ \ &(1 - t)(\quad u) F(s,0,1) \\
+ \ &(\quad t)(1 - u) F(s,1,0) \\
+ \ &(\quad t)(\quad u) F(s,1,1)
\end{aligned}
$$

$$
\begin{aligned}
P_u P_s = \ &(1 - u)(1 - s) F(0,t,0) \\
+ \ &(1 - u)(\quad s) F(1,t,0) \\
+ \ &(\quad u)(1 - s) F(0,t,1) \\
+ \ &(\quad u)(\quad s) F(1,t,1)
\end{aligned}
$$

$$P_s P_t P_u = \begin{aligned} &(1 - s) (1 - t) (1 - u) \; F(0,0,0) \\ + \; &(1 - s) (1 - t) (\quad u) \; F(0,0,1) \\ + \; &(1 - s) (\quad t) (1 - u) \; F(0,1,0) \\ + \; &(1 - s) (\quad t) (\quad u) \; F(0,1,1) \\ + \; &(\quad s) (1 - t) (1 - u) \; F(1,0,0) \\ + \; &(\quad s) (1 - t) (\quad u) \; F(1,0,1) \\ + \; &(\quad s) (\quad t) (1 - u) \; F(1,1,0) \\ + \; &(\quad s) (\quad t) (\quad u) \; F(1,1,1) \end{aligned}$$

The relation between the interpolation variables s, t, and u and the grid generation variables I, J, and K are:

$$s = (I - 1) / (I_{max} - 1)$$

$$t = (J - 1) / (J_{max} - 1)$$

$$u = (K - 1) / (K_{max} - 1).$$

APPENDIX E

2-D Grid Generation Code Input Directions

Note: all data is in free format
Note: Cards 2, 4, 6, 10, 14, 19 and 22 are data set header cards and must be input as indicated; i.e., data is not entered on those cards.

Card #

1.   title

2.   MI MJ MK #ITER SIGMA TOC R

3.   mi mj mk #iter sigma toc r

mi = number of grid pts in the I direction

mj = number of grid pts in the J direction

mk = number of grid pts in the K direction

#iter = number of iteration

sigma = spline fit coefficient

0 → cubic spline fit
+ ∞ → straight line fit

toc = percent increase of input airfoil coordinates

1 → no change to input coordinates

r = relaxation factor, 0 < r < 2 (1.1 has been used with some success)

4.   T1 T2 T3 T4 T5 T6 T7 T8 T9 T10 T11

5.   t1 t2 t3 t4 t5 t6 t7 t8 t9 t10 t11

t1 = percent of root chord arch length for the leading grid point spacing on the root chord.

t2 = percent of root chord arch length for the trailing grid point spacing on the root chord.

t3 = spanwise trailing-edge grid spacing at the tip, ratioed to t1; t3 = 1. will cause leading spacing to be constant from root to tip.

t4 = spanwise trailing-edge grid spacing in percent semispan at the root chord.

47

t5 = leading edge root chord stand-off distance of J = 2 layer, in percent root chord.

t6 = far-field grid spacing along J line extending through root chord leading edge, in percent root chord.

t7 = distance from leading edge root chord to far field in percent root chord.

t8 = tip spanwise stand-off distance of J = 2 layer, in percent root chord.

t9 = spanwise grid spacing at the far field on the trailing edge grid, in percent root chord.

t10 = distance spanwise from wingtip trailing edge to far field, in percent root chord.

t11 = vertical distance from root chord trailing edge to far field, in percent root chord.

6.   LEADING-EDGE SHAPE

7.   #lepts
     #lepts = number of points defining wing's leading edge and tip.

8. y_1 y_2 ... y_n

     spanwise coordinates of points describing the wingtip and leading edge, from wingtip trailing edge to leading-edge root chord.

9. x_1 x_2 ... x_n

     spanwise coordinates of points describing the wing tip and leading edge, from wing tip trailing edge to leading edge root chord.

10. TRAILING-EDGE SHAPE

11. #tepts

12. y_1 y_2 ... y_n

     spanwise coordinates of points describing the wing trailing edge, from root to tip.

13. x_1 x_2 ... x_n

     spanwise coordinates of points describing the wing trailing edge, from root to tip.

14. UPPER SURFACE AIRFOIL DATA

48

15.   ninsecu

           ninsecu = number of airfoil sections describing the wing upper
               surface.

16.   AIRFOIL SECTION IDENTIFIER

17.   nptsec xlesec ylesec xtesec ytesec

           nptsec = number of data points describing the airfoil section.

           xlesec, ylesec = the streamwise and spanwise coordinates of the
                                   section leading edge.

           xtesec, ytesec = the streamwise and spanwise coordinates of the
                                   section trailing edge.

18.   − x_1 z_1

                x_2 z_2

                x_3 z_3

                .   .

                .   .

                .   .

            x_{NPTSEC} z_{NPTSEC}

           airfoil section coordinates nondimenionalized by local chord,
             leading edge x = 0.
             trailing edge x = 1. or 100.

    Repeat cards 16, 17, and 18 NINSECU times to enter all upper surface
      airfoil sections.

19.   WINGTIP SHAPE
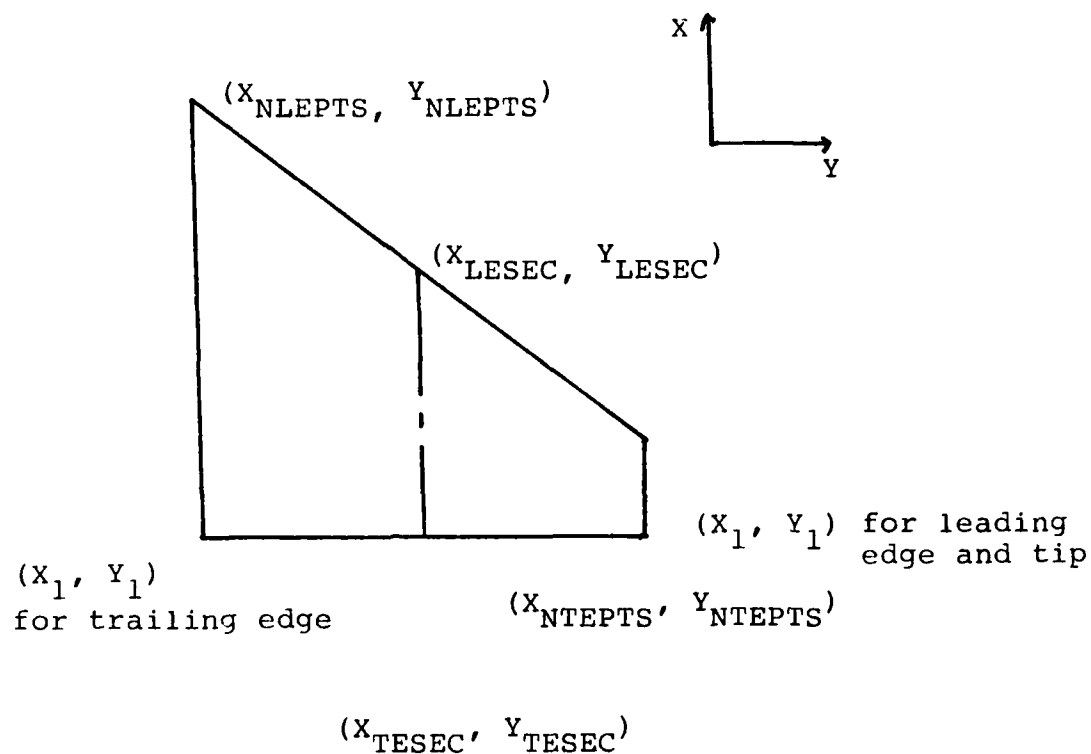
20.   npttip = number of points describing the true wingtip (zero
                           thickness) camber shape.

21. x_1 z_1

                x_2 z_2

                .   .

                .   .

                .   .

            x_{npttip} z_{npttip}

22.   LOWER SURFACE AIRFOIL DATA

23.   ninsecl

Repeat cards 16, 17, and 18 NINSECL times to enter all lower surface airfoil sections.
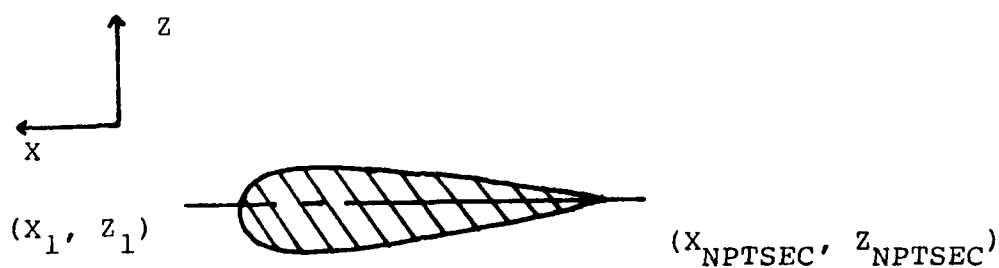
PLANFORM INPUTS

AIRFOIL SECTION INPUTS

Figure E1. Input Data Definitions